Quantitative proteomic analysis of the association between decreasing *O*-GlcNAcylation and metastasis in MCF-7 breast cancer cells

PUKKAVADEE NETSIRISAWAN[1], DARANEE CHOKCHAICHAMNANKIT[1], KITTIRAT SAHARAT[1], CHANTRAGAN SRISOMSAP[1], JISNUSON SVASTI[1,2] and VORARATT CHAMPATTANACHAI[1,2]

[1]Laboratory of Biochemistry, Chulabhorn Research Institue and [2]Applied Biological Sciences Program, Chulabhorn Graduate Institute, Bangkok 10210, Thailand

Received August 5, 2019; Accepted February 6, 2020

DOI: 10.3892/ijo.2020.5022

Abstract. Breast cancer is the most common type of cancer and leading cause of cancer-associated mortality in women worldwide. O-linked N-acetyl glucosaminylation (*O*-GlcNAcylation) is a dynamic post-translational modification of nuclear, cytoplasmic and mitochondrial proteins. Mounting evidence suggests that abnormal *O*-GlcNAcylation status is associated with cancer malignancy. In our previous study, it was reported that *O*-GlcNAc and *O*-GlcNAc transferase (OGT; an enzyme responsible for the addition of *O*-GlcNAc) were upregulated in breast cancer tissues and cells. Moreover, *O*-GlcNAcylation was required for resistance to anoikis and the anchorage-independent growth of breast cancer cells. However, the precise roles of this modification on the development of malignancy are yet to be elucidated. Therefore, in the present study, the effects of inhibiting *O*-GlcNAc on the malignant transformation of MCF-7 breast cancer cells under different culture conditions were determined, using monolayer (primary growth), anoikis resistance (spheroid growth) and reseeding (secondary growth) to mimic the metastatic process. Decreasing *O*-GlcNAc levels using small interfering (si)RNA targeting OGT resulted in a reduction in cell viability and invasiveness in anoikis resistant and reseeding conditions. Furthermore, gel-free quantitative proteomics was performed to identify the proteins affected by a reduction of *O*-GlcNAc. A total of 317 proteins were identified and compared, and the expression of 162 proteins was altered >1.5 fold in the siOGT treated cells compared with the siScamble (siSC) treated cells. Notably, 100 proteins involved in cellular metabolism, cellular localization, stress responses and gene expression were significantly altered in the reseeding condition. Among these differentially expressed proteins, the levels of small nuclear ribonucleoprotein Sm D1 exhibited the largest decrease in expression following knockdown of OGT, and this reduction in expression was associated with a significant decrease in the levels of mTOR expression, a protein which promotes tumor growth and progression. Taken together, the results of the present study demonstrate that decreasing *O*-GlcNAcylation altered protein expression, and ultimately influenced the metastatic processes, particulary regarding the invasion and reattached growth of MCF-7 breast cancer cells.

Correspondence to: Dr Voraratt Champattanachai, Laboratory of Biochemistry, Chulabhorn Graduate Institute, 54 Kamphaeng Phet 6, Laksi, Bangkok 10210, Thailand
E-mail: voraratt@cri.or.th

Key words: breast cancer, metastasis, *O*-GlcNAcylation, quantitative proteomics, protein networking

Introduction

The 2018 status report on the global cancer statistics showed that breast cancer is the most common type of cancer and leading cause of cancer-associated mortality affecting women worldwide (1). If detected in the early stages, breast cancer is curable; however, the majority of patients with breast cancer are diagnosed at the first instance with advanced stage breast cancer, which is associated with a less favorable prognosis and decreased survival times (2). Tumor metastasis, or the spread of cancer cells throughout the body, accounts for a large number of cancer-associated deaths, and it has been estimated to account for ~90% of all cancer-associated mortalities worldwide (3). Therefore, a considerable body of research has been performed to determine the mechanisms underlying the metastatic process and the complex interactions between cancerous cells, surrounding healthy cells and the tumor microenvironment. During malignant transformation, malignant tumors at the primary site (primary cancer cells) penetrate through the basement membranes and extracellular matrix to invade adjacent tissues, metastasize and are then transported via the circulatory system (circulating cancer cells). Finally, these metastatic cells extravasate, attach to a distant tissue, proliferate and form a new distant tumor (secondary cancer cells) (4). Nowadays, ongoing research has focused on identifying and understanding the mechanisms of cancer metastasis which may result in the more efficient treatment of patients with metastatic cancer (5).

Altered metabolism is a hallmark of cancer cells, as illustrated by the Warburg effect; a phenomenon that demonstrates

the increased rate of glucose consumption and utilization of the glycolytic pathway in cancer cells, even in the presence of oxygen (6). This metabolic shift can alter glucose metabolism to produce the energy and biological macromolecules required for cancer cell growth and proliferation. One of the metabolic shifts includes the hexosamine biosynthesis pathway (HBP), a minor branch of the glycolytic pathway. The end product of HBP is uridine diphosphate N-acetylglucosamine (UDP-GlcNAc), a sugar donor for post-translational protein modifications, including classical glycosylation occurring in the endoplasmic reticulum and golgi apparatus and *O*-linked N-acetyl glucosaminylation (*O*-GlcNAcylation), which occurs in the cytoplasm, nucleus and mitochondria (7). The latter glycosylation type is dynamically regulated by two key enzymes, *O*-GlcNAc transferase (OGT) (8) and *O*-GlcNAcase (9), which are responsible for the addition and removal of *O*-GlcNAc from target proteins, respectively. Growing evidence has suggested that abnormal *O*-GlcNAcylation status is associated with cancer malignancy (10,11).

In our previous studies, it was demonstrated that *O*-GlcNAcylation was increased in primary breast and colorectal cancer tissues (12,13). Moreover, *O*-GlcNAcylation is required for anoikis resistance and anchorage-independent growth, which are vital steps in the progression of breast cancer (14). However, the precise roles of this modification regarding malignant transformation are yet to be elucidated. Therefore, in the present study, the effects of *O*-GlcNAc inhibition on the malignant transformation of MCF-7 breast cancer cells under different culture conditions were determined, using monolayer (primary growth), anoikis resistance (spheroid growth) and reseeding (secondary growth) to mimic the metastatic processes. As *O*-GlcNAc-modified proteins have been reported to influence breast cancer cell progression and metastasis, several biological effects of *O*-GlcNAc reduction in MCF-7 cells were investigated by assessing cell morphology, viability and invasiveness under different culture conditions. Furthermore, gel-free quantitative proteomics coupled with LC-MS/MS analysis were used to identify proteins affected by *O*-GlcNAc inhibition, which may serve important roles in cancer metastasis.

Materials and methods

Breast cancer cell line. MCF-7 breast cancer cells were purchased from the American Type Culture Collection and cultured in DMEM (Gibco; Thermo Fisher Scientific, Inc.) containing 10% FBS (Hyclone Laboratories; GE Healthcare Life Sciences), 100 U/ml penicillin and 100 mg/ml streptomycin (both Gibco; Thermo Fisher Scientific, Inc.).

Transfection of siRNA. Stealth RNAi oligonucleotides against OGT (siOGT) and scrambled negative control medium GC duplex (siSC; cat. no. 12935300), were purchased from Invitrogen (Thermo Fisher Scientific, Inc.) and used according to the manufacturer's protocol. The forward and reverse sequences of siOGT were 5'-UAAUCAUUUCAAUAACUG CUUCUGC-3' and 5'-GCAGAAGCAGUUAUUGAAAUG AUUA-3', respectively. To silence *OGT* expression using RNA interference, $2x10^5$ cells were suspended in 2 ml antibiotic-free DMEM and added to 6-well plates (conventional plate for monolayer condition and poly-HEMA coated plate for anoikis induction). Subsequently, cells in all conditions were transfected with 20 nM stealth siOGT or scramble negative control using Lipofectamine® 2000 reagent (Invitrogen; Thermo Fisher Scientific, Inc.), according to the manufacturer's instructions, and cultured for 3 days in a humidified incubator with 5% CO_2 at 37˚C.

In vitro model of metastasis. Metastasis was assessed *in vitro* by culturing cells in three different conditions to determine the effect of *O*-GlcNAcylation inhibition on MCF-7 breast cancer cells. The first condition was as a monolayer culture (used to mimic breast cancer cells at the primary site), where MCF-7 cells were plated in conventional culture containers and transfected with small interfering RNA (siRNA) against OGT or scrambled siRNA control for 3 days in a humidified incubator with 5% CO_2 at 37˚C. The second condition was the anoikis resistant culture (spheroid formation) which was used to mimic breast cancer cells which are transported via the circulatory system. To induce anoikis, cells were plated in 6 well-plates pre-coated at 37˚C for 1 day with poly-2-hydroxyethyl methacrylate (poly-HEMA; Sigma-Aldrich; Merck KGaA) and cultured for 3 days in an incubator as mentioned above. The poly-HEMA-coated plates were prepared as previously described (15). Briefly, 2 ml of poly-HEMA (30 mg/ml solution) was dissolved in 95% ethanol, added to the 6 well-plates and dried completely at 37˚C in an incubator, followed by UV sterilization before use in subsequent experiments. The final condition was re-attachment or reseeding (used to mimic breast cancer cells at the secondary site). Spheroid cells transfected with siOGT or siSC for 3 days were harvested and washed with 1 ml PBS and centrifuged at 1,000 x g at 4˚C for 5 min. Cell pellets were treated with trypsin at 37˚C for 10 min and resuspended in 1 ml DMEM. Subsequently, $1x10^6$ cells were reseeded in T-25 flasks for the reseeding condition, and further incubated for another 3 days in an incubator, in the aforementioned conditions.

Cellular morphology, cytoplasmic vacuolation and growth assay. MCF-7 breast cancer cells from all culture conditions were observed after culturing using an inverted microscope (Eclipse TS100; Nikon Corporation) and then imaged using an attached D5100 camera (Nikon Corporation). Furthermore, the accumulation of cytoplasmic vesicles in MCF-7 cells in the reseeding culture condition were counted. At least 5 random fields (magnification, x400) were imaged and the number of cytoplasmic vacuoles were counted in each field. The vacuole sizes were determined using ImageJ (version 1.42I; National Institutes of Health). These were classified into two groups according to their size; microvacuoles ($\leq$50 μm) and macrovacuoles ($\geq$50 μm). The average number of micro and macrovacuoles was calculated in the siSC control and siOGT cells, and the assay was repeated three times. Subsequently, the viability of transfected cells was assessed using the trypan blue dye exclusion assay. The number of viable and non-viable cells from 4 fields of view were counted using a hemocytometer with 0.4% trypan blue (1:1 volume/volume) at room temperature within 10 min, and the assay was repeated three times. Results are presented as the mean ± standard deviation of viable cells in the OGT knockdown group, normalized to those in the siSC group.

In vitro cell invasion assay. The invasion of transfected cells in monolayer, anoikis resistant and reseeding conditions were assayed in modified Boyden chambers as described previously, with certain modifications (16). Briefly, for the invasion assay, 8-μm pore membrane filters were placed in Transwell chambers (Corning, Inc.) and the upper chamber was coated with 30 μg Matrigel (BD Biosciences) at 37˚C in an incubator overnight. A suspension of $2x10^5$ cells from each culture condition was added to the upper chamber (200 μl/chamber), and DMEM was added to the lower chamber (500 μl/chamber). The chamber was incubated at 37˚C for 24 h in a humidified atmosphere of 5% CO_2. Subsequently, the cells on the upper surface were removed with a cotton swab, and the cells were fixed with 30% methanol, followed by staining with 0.5% crystal violet in 20% methanol, both steps were performed for 15 min at room temperature. Finally, stained cells were counted in 5 randomly selected fields, using an inverted microscope (Eclipse TS100; Nikon Corporation) and then imaged using an attached D5100 camera (Nikon Corporation) (magnification, x100).

In-solution trypsin digestion. Cultured cells were resuspended in a digestion solution (50 mM ammonium bicarbonate) and sonicated until the turbid suspensions became clear. Sonicated samples were centrifuged at 10,000 x g, 4˚C for 10 min and protein concentration was determined using a Bio-Rad Protein assay (Bio-Rad Laboratories, Inc.). A total of 10 μg of each sample was reduced with 10 mM DTT at 37˚C for 1 h, followed by an alkylation step with 30 mM iodoacetamide in the dark at room temperature for 30 min. Subsequently, samples were digested in solution overnight with 0.2 μg trypsin (Promega Corporation) at 37˚C. After digestion, samples were acidified with formic acid and then desalted using C18 ZipTips (EMD Millipore) at room temperature for 10 min.

Liquid chromatography-mass spectrometry (LC-MS) analysis. Digested peptides were identified using nanoflow liquid chromatography coupled with amaZon speed ion trap mass spectrometry (Bruker-Michrom, Inc.), as previously described (17). The peptides were concentrated and desalted on a 75-umidx200 mmC18 Easy-nLC™ column (Thermo Fisher Scientific, Inc.). The mass spectrometer was operated in positive ion mode with a CaptiveSpray ion source and a spray voltage of 1,500 v, dry temperature of 150˚C, without nebulizer gas and a mass range between 400-1,400 m/z. The parameter was optimized at 922 m/z with an ion charge count target of 400,000. To elute peptides, 0.1% formic acid in 3% acetonitrile (solution A) and 0.1% formic acid in 97% acetonitrile (solution B) were used with the following conditions: 10-70% B at 0-70 min, 90% B at 70-75 min and 10% B at 75-90 min. The raw data were processed using Bruker compass version 1.4 (Bruker-Michrom, Inc.). DataAnalysis™ version 4.0 (Bruker-Michrom, Inc.) created Mascot compatible files (mgf) to facilitate Mascot database searches. Each sample was assessed three times.

Protein quantification and identification. Progenesis QI (version 3.1; Nonlinear Dynamics), a label-free quantitative LC-MS software, was used to identify and quantify differential protein expression between siSC and siOGT treated cells in each of the three culture conditions. In total, 6 samples were analyzed using LC-MS/MS each in triplicate: siOGT and siSC MCF-7 cells of monolayer, anoikis resistant and reseeding conditions. The chromatograms of all samples were aligned and the sample with the smallest differences in retention times and MS peaks among all the samples was selected as the reference. The ion intensities of MS peaks of each sample were then normalized to those of the established reference. Obtained MS/MS spectra from Progenesis QI were used to perform peptide searches using the Mascot search engine against the SwissProt database (http://www.matrixscience.com/) (18). Search parameters of MS/MS data included trypsin protease specificity with the possibility of one missed cleavage, peptide/fragment mass tolerances of 0.6 Da and fixed modifications of carbamidomethylation at cysteine and oxidation at methionine. Significant peptide identifications above the identity or homology threshold were adjusted to ≤1% peptide false discovery rate using the Mascot Percolator algorithm (19).

Relative quantitation of the normalized abundance of each peptide was performed by selecting only non-conflicting unique peptides with a Mascot ion score >30 ($P<0.05$). Furthermore, the identified peptides were further filtered using the following criteria: Peptides exhibiting $P\leq0.01$ between the triplicate runs ANOVA and with spectral counts ≥2 across the three technical replicates in all samples. Subsequently, MS ion intensities of each individual confident peptide derived from the same protein were combined and averaged. The normalized values of protein expression levels (combined MS ion intensities of confident peptides) of each sample were calculated by dividing by the lowest value of those protein levels among the 6 samples. The expression levels of each protein were calculated as the ratio (+/-) of the average MS ion intensities between siSC and OGT knockdown of monolayer, anoikis resistant and reseeding conditions. (+) signifies the intensity in OGT knockdown is higher compared with the siSC, whereas (-) indicates the band intensity in OGT knockdown is lower compared with the siSC treated group.

Heat map analysis of protein expression patterns in the monolayer, anoikis resistant and reseeding conditions. To obtain relative protein abundance measurements from Progenesis QI, fold changes of protein expression levels between siOGT and siSC treated cells of the three conditions were compared. Subsequently, heat map analysis of protein expression levels was performed using R-software (r-project.org; version 3.3.1) via the pheatmap package (https://cran.r-project.org/web/packages/pheatmap/index.html). Proteins were clustered according to their expression levels using the following parameters: Distance computational method, Minkowski and agglomeration method, Complete.

Determining protein-protein interactions. The online tool Search Tool for the Retrieval of Interacting Genes/Proteins (STRING; string-db.org; version 11.0) was used to construct interactome maps of differential proteins. The indicated network properties included: Nodes, number of proteins in the network; edges, number of interactions; node degree, average number of interactions; and clustering coefficient, tendency of the network to form clusters. The closer the local clustering coefficient was to 1, the more likely it was for the network to form clusters; PPI enrichment P-value, statistical significance.

Western blotting. Cells were lysed in RIPA buffer containing 1% protease inhibitor cocktail (both Sigma-Aldrich; Merck KGaA) and 20 μM Thiamet-G (Sigma-Aldrich; Merck KGaA), an *O*-GlcNAcase inhibitor. Protein concentrations were measured using a Bio-Rad Protein assay (Bio-Rad Laboratories, Inc.). Protein samples (30 μg/lane) were loaded on a 10% SDS-gel, resolved using SDS-PAGE and transferred to PVDF membranes (EMD Millipore). The levels of *O*-GlcNAc, OGT and β-actin were determined using western blotting with primary antibodies, including antibodies against *O*-GlcNAc-modified proteins RL2 (1:1,000; cat. no. ab2739; Abcam), OGT (1:1,000; cat. no. O6264; Sigma-Aldrich; Merck KGaA) and β-actin (1:10,000; cat. no. mAb3700; Cell Signaling Technology, Inc.), with overnight incubation at 4˚C in 1% PBS-casein blocking buffer (Bio-Rad Laboratories, Inc.) as previously described (14). The membranes were incubated with the corresponding secondary antibodies, including swine anti-rabbit (1:5,000; cat. no. P-0217; Dako; Agilent Technologies, Inc.) for OGT and rabbit anti-mouse immunoglobulins (1:5,000; cat. no. P-0260; Dako; Agilent Technologies, Inc.) for RL2 and β-actin, respectively. Western blots were developed using WesternBright™ enhanced chemiluminescent reagent (Advansta, Inc.) and visualized using ImageQuant LAS4000 (GE Healthcare). β-actin was used as the loading control.

The expression of epithelial-mesenchymal transition (EMT) markers were also assessed using western blotting with antibodies against β-catenin (cat. no. mAb9582), E-cadherin (cat. no. mAb3195) and N-cadherin (cat. no. mAb4061) (all 1:1,000; Cell Signaling Technology, Inc.). All membranes were incubated with goat anti-rabbit immunoglobulins (1:5,000; cat. no. 7074; Cell Signaling Technology, Inc.) secondary antibody and the detection was performed, as described previously (14).

The expression levels of representative proteins were validated by western blotting using the following antibodies; monoclonal mouse anti-human nucleophosmin (NPM1; 1:1,000; cat. no. ab55708; Abcam), monoclonal mouse anti-human heat shock protein 27 (HSP27; 1:2,000; cat. no. ab2790; Abcam), monoclonal rabbit anti-human small nuclear ribonucleoprotein Sm D1 (SNRPD1; 1:5,000; cat. no. ab50940; Abcam), monoclonal rabbit anti-human Histone H3 (1:1,000; cat. no. mAb9715; Cell Signaling Technology, Inc.), monoclonal mouse anti-human cytokeratin18 (1:10,000; cat. no. MAB3236; Chemicon; Thermo Fisher Scientific, Inc.) and monoclonal rabbit anti-human mTOR antibody (1:1,000; cat. no. mAb2972; Cell Signaling Technology, Inc.). The membranes were incubated with the appropriate secondary antibodies, including swine anti-rabbit (1:5,000; cat. no. P-0217; Dako; Agilent Technologies, Inc.) for SNRPD1, Histone H3 and mTOR and rabbit anti-mouse immunoglobulins (1:5,000; cat. no. P-0260; Dako; Agilent Technologies, Inc.) for NPM1, HSP27 and CK18, respectively. Then, the detection was performed as described above. The results were reported as the average band intensity ± standard deviation of proteins of interest in the OGT knockdown cells normalized by to the intensity of the siSC. In certain experiments, the protein expression ratios (+/-) were calculated from band intensities of proteins of interest between siSC and OGT knockdown. (+) means the intensity in OGT knockdown is higher than that in siSC whereas (-) indicates the band intensity in OGT knockdown is lower than that of the siSC, respectively. At least three independent experiments were performed.

Statistical analysis. Statistical comparisons between two groups were performed using a one-sample paired Student's t-test and a one-way ANOVA was used followed by a Bonferroni's multiple comparison test to compare differences between multiple groups. All analyses were performed using GraphPad Prism version 5.0 (GraphPad Software, Inc.). $P<0.05$ was considered to indicate a statistically significant difference.

Results

Transient knockdown of O-GlcNAc transferase influences O-GlcNAc and OGT expression which alters cell morphology, vacuole numbers and cell viability. As *O*-GlcNAcylation and OGT levels were upregulated in numerous cancer cell lines, transient knockdown of *O*-GlcNAcylation by RNA interference against OGT was performed under different culture conditions. siOGT transfection in all conditions significantly decreased both OGT and *O*-GlcNAcylation levels compared with the respective siSC group (Fig. 1A).

After that, cellular morphology under different culture conditions were examined. OGT knockdown and siSC cells exhibited normal cellular morphology in the monolayer conditions (Fig. 1B). For the anoikis resistant model, detached siSC and siOGT MCF-7 cells spontaneously aggregated into spheroid bodies, but there was no difference in morphology between the two groups (Fig. 1B). However, when these spheroid cells were reseeded in the attachment culture, the siSC cells adhered well, displaying a normal morphology. By contrast, the siOGT treated cells demonstrated notable morphological changes with an increase in the number of cytoplasmic vacuoles of varying sizes. The cytoplasmic vacuolation was assessed and the total amount of macrovacuoles in siSC cells was 10%; whereas in OGT silenced cells, the total proportion of macrovacuoles was increased to 25% (Fig. 1B). Therefore, OGT knockdown may serve a pivotal role in cellular morphology, particularly in the reseeding condition (Fig. 1B). Subsequently, it was determined whether decreasing *O*-GlcNAcylation levels affected cell viability of MCF-7 cells under different culture conditions. Using a trypan blue exclusion assay, the results indicated a significant reduction in cell viability in the siOGT transfected MCF-7 cells, in both the anoikis resistant and reseeding conditions ($P<0.01$); however, this phenomenon was not observed in the monolayer culture (Fig. 1C). Therefore, OGT and *O*-GlcNAc may serve a role in cell reseeding, which is representative of cancer cells metastasizing to the secondary sites.

OGT is required for cancer invasion. To determine whether decreasing *O*-GlcNAcylation levels affected invasion of MCF-7 cells, an *in vitro* cell invasion assay was performed using Boyden chambers. As revealed in Fig. 2A, reducing *O*-GlcNAcylation levels had no significant effect on the invasiveness of cells in the cultured monolayer conditions, and significantly inhibited invasion of the anoikis resistant and reseeding conditions (Fig. 2A). Transient OGT knockdown

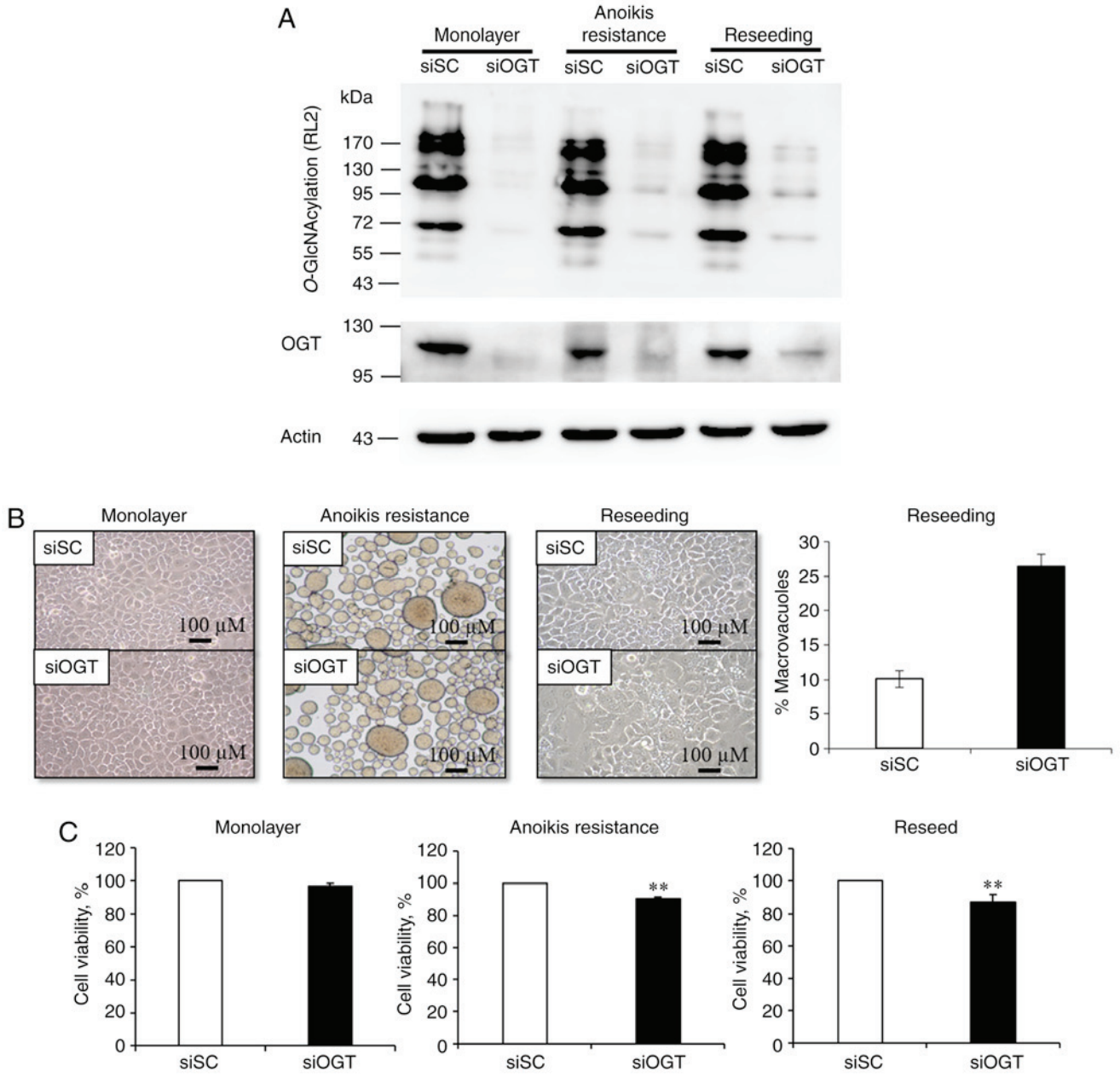

Figure 1. Effects of the decreased of *O*-GlcNAcylation and OGT expression levels on cell morphology and viability under monolayer, anoikis resistant and reseeding conditions. MCF-7 cells were transiently transfected with siOGT or siSC and cultured under the specific conditions. (A) Expression levels of *O*-GlcNAcylation and OGT were determined by western blotting, with β-actin as the loading control. (B) Representative images of cells cultured under different conditions. Magnification, x100. Graphs represent the percentage of macrovacuoles in reseeding condition. (C) Graphs represent the percentage of viable cells in each condition normalized to the siSC group. Cell viability was determined using a trypan blue exclusion assay. Data are presented as the mean ± standard deviation of three independent experiments. **P<0.01 vs. siSC. SC, scramble; OGT, *O*-GlcNAc transferase; si, small interfering.

resulted in a significant decrease of invasion in the anoikis resistant (>80%) and reseeding conditions (>90%), respectively, compared with the siSC (Fig. 2B). These data suggest that aberrant OGT and *O*-GlcNAc levels may contribute to cancer invasion, under anoikis resistant and reseeding conditions. Furthermore, to clarify whether the effects of OGT and *O*-GlcNAcylation on MCF-7 breast cancer cells was associated with EMT, the expression of EMT markers including E-cadherin, N-cadherin and β-catenin were assessed. However, there was no significant difference in the expression of EMT-associated proteins between the siSC and siOGT knockdown cells in all culture conditions (Fig. S1). Therefore, OGT does not appear to regulate EMT.

Knockdown of OGT alters global protein expression in the anoikis resistant and reseeding conditions. To examine differential protein expression in response to decreasing *O*-GlcNAcylation levels under different culture conditions, label-free quantitative proteomics coupled with LC-MS/MS analysis was used. A total of 317 differentially expressed proteins were identified and compared between the 6 sample groups (siOGT vs. siSC treated cells in monolayer, anoikis resistant and reseeding conditions), but only 162 proteins had a fold-change in expression >1.5 in the siOGT compared with the siSC treated cells. The protein fold change of each condition is represented by the ratio of protein levels in the siOGT relative to siSC (upregulation, +) or siSC relative to siOGT (downregulation, -). As indicated in Fig. 3A,

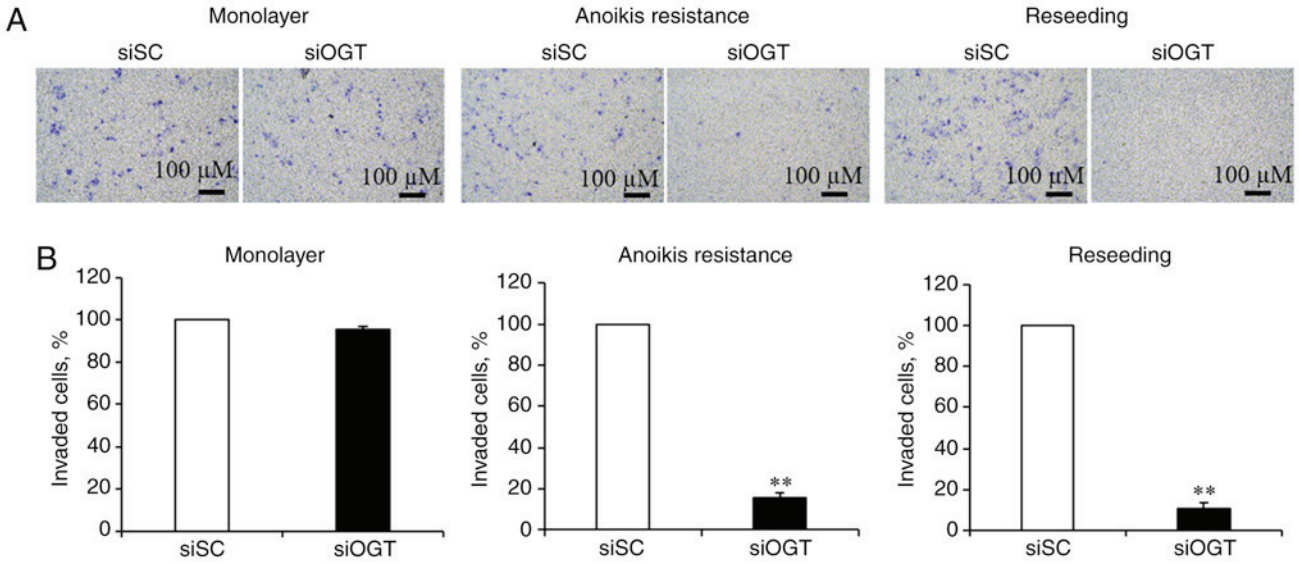

Figure 2. Effects of OGT knockdown on cancer cell invasiveness under monolayer, anoikis resistant and reseeding conditions. Cells were transfected with siOGT or siSC and cultured in monolayer, anoikis resistant or reseeding conditions. (A) Representative pictures of invaded MCF-7 cells. (B) Quantitative analysis of invaded cells normalized to the siSC group. Data are presented as the mean ± standard deviation of at least three independent repeats. **P<0.01 vs. siSC. OGT, *O*-GlcNAc transferase; si, small interfering.

heat map data revealed that there was a trend in changes in protein expression reflecting the particular culture conditions. The results revealed OGT silencing markedly altered cell biological effects only in the anoikis resistant and reseeding conditions. A heat map of the top 20 proteins (10 upregulated and 10 downregulated) differentially expressed in anoikis resistant and reseeding conditions was generated (Fig. 3B and C, respectively). The two heat maps represent the protein expression levels of individual samples (in triplicate) between the siSC and siOGT cells. According to the heat map analysis, a notable decrease in the expression of specific proteins in the reseeding condition was observed. Using a threshold of >1.5-fold change in expression levels between siOGT and siSC treated cells, there were 78 upregulated and 1 downregulated protein in the monolayer condition, 67 upregulated and 5 downregulated proteins in the anoikis resistant condition and 13 upregulated and 85 downregulated proteins in the reseeding condition. A total of 162 unique proteins exhibited >1.5 fold difference in expression levels between siOGT and siSC transfected cells in ≥1 culture condition (Table I). Notably, the changes in the expression of certain proteins were consistent with regards to up- or down-regulation, whereas other proteins exhibited culture-specific expression changes. The data were re-analyzed and presented in a Venn diagram in order to display the unique number of proteins affected in each condition (Fig. 3D). As only anoikis resistant and reseeding conditions exhibited significant changes in biological effects following OGT knockdown, a focus was placed on differentially expressed proteins in these two conditions. The Venn diagram demonstrated 21 and 46 proteins expressed predominantly in anoikis resistant and reseeding conditions, respectively, and 54 unique proteins were differentially expressed in ≥1 of the culture conditions.

Prediction of protein-protein interactions and roles of potential proteins in breast cancer metastasis. The results of the present study indicate that OGT serves pivotal roles in cell viability and invasion in MCF-7 cells only in anoikis resistant and reseeding conditions. Thus, the potential protein interactions were predicted using STRING. STRING analysis was performed on the 121 proteins derived from the Venn diagram which were only expressed in anoikis resistant and reseeding conditions, and the proteins that were differentially expressed only in the monolayer condition were excluded. The protein-protein interaction networks were separated into three groups according to their expression conditions: Proteins differentially expressed only in the anoikis resistant condition (21 proteins); proteins differentially expressed only in the reseeding conditions (46 proteins); and unique proteins differentially expressed in either anoikis resistant or reseeding conditions (54 proteins). The results from STRING were analyzed according to the biological functions of proteins. The analysis indicated that the majority of proteins derived from the anoikis resistant group were clustered into one major group which was involved in cellular metabolism (red background) as indicated in Fig. 4A. Examples of proteins in this group included 3-hydroxyacyl-CoA dehydrogenase type-2, ATP-citrate synthase and 4-aminobutyrate aminotransferase. In addition, the differentially expressed proteins in the reseeding group were predominantly clustered into one of three groups (Fig. 4B). The first group (red background) was involved in cellular metabolism, and included as histone H3, glucosidase 2 subunit β and fatty acid synthase. The second group (green background) was associated with cellular localization and included nuclear matrix protein 1, 14-3-3 protein γ and tubulin α-1B chain. The final group (orange background) was involved with stress responses and included HSP-β1, HSP27, annexin A5 and Serpin H1. The differentially expressed proteins observed in both anoikis resistant and reseeding conditions were clustered into three main groups, as displayed in Fig. 4C. The first group (red background) was primarily involved in cellular metabolism, and included SNRPD1, acetyl-CoA acetyltransferase and

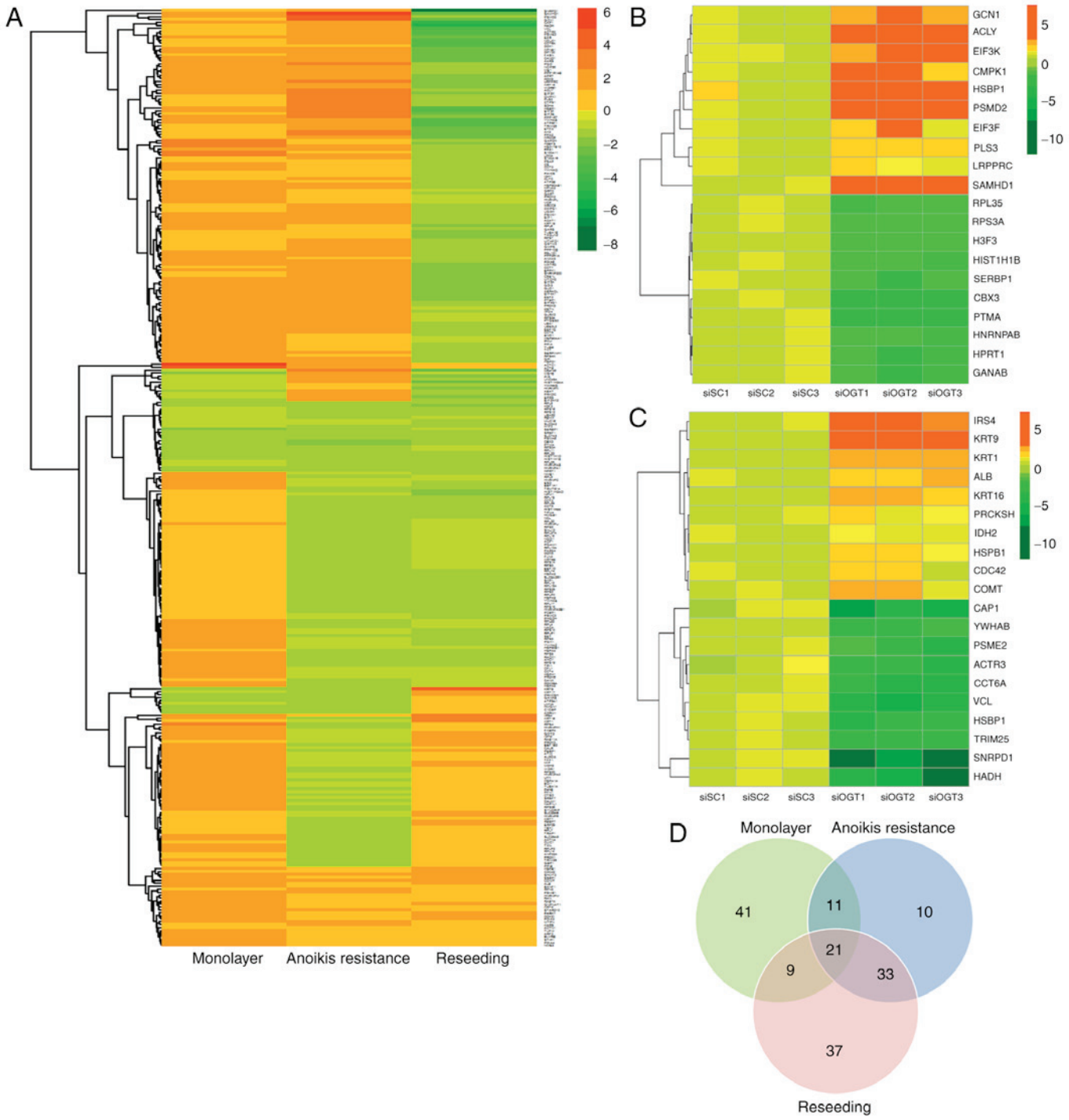

Figure 3. Heat map and Venn diagram of differential protein expression signatures. (A) Heat map of all 317 proteins derived from label-free quantitative proteomic analysis, based on the average of three replicate runs under different culture conditions. Differential protein expression was derived by the protein expression level ratio between siOGT vs. siSC treated cells. Each column represents a specific culture condition and each row represents a protein. The numbers on heat map represent protein fold change ratio of siOGT relative to siSC (upregulation, +) or siSC relative to siOGT (downregulation, -). Heat map of the top 20 differentially expressed proteins in (B) anoikis resistant and (C) reseeding conditions of siSC or siOGT transfected cells, according to three replicate samples. Each column represents the protein expression levels and each row represents a protein. The numbers on heat map represent protein expression levels. (D) Venn diagram of proteins with >1.5 fold differential expression between siOGT and SiSC cells under monolayer, anoikis resistant and reseeding conditions. OGT, *O*-GlcNAc transferase; si, small interfering; SC, Scramble.

catechol *O*-methyltransferase. The second group (green background) was associated with cellular localization and included keratin, type I cytoskeletal (CK)18, CK19 and ezrin. The final group (blue background) was associated with gene expression regulation, and included elongation factor 2, eukaryotic initiation factor 4A-I and eukaryotic translation initiation factor 1.

Validation of proteins of interest associated with cancer metastasis. A total of 121 proteins exhibited >1.5-fold

Table I. Lists of proteins that showed increase or decrease their protein expression levels with the changes of more than 1.5 fold between siOGT versus siSC treated cells at least in one of three culture conditions.

Protein name	Protein accession	Relative protein expression levels									ANOVA P-value	Protein score	Identified peptides
		Monolayer			Anoikis resistance			Reseeding					
		si SC	si OGT	Ratio	si SC	si OGT	Ratio	si SC	si OGT	Ratio			
14-3-3 protein beta/alpha	1433B_HUMAN	2.50	3.64	1.5	1.08	2.31	2.2	2.90	1.00	-2.9	$1.52x10^{-5}$	573	8
14-3-3 protein gamma	1433G_HUMAN	2.18	2.08	-1.1	1.00	1.11	1.1	1.80	1.12	-1.6	$3.31x10^{-3}$	233	4
26S protease regulatory subunit 4	PRS4_HUMAN	1.19	1.99	1.7	1.00	1.72	1.7	2.06	1.35	-1.5	$5.43x10^{-3}$	41	1
26S proteasome non-ATPase regulatory subunit 2	PSMD2_HUMAN	1.87	3.61	1.9	1.00	4.19	4.2	2.95	2.34	-1.3	$1.73x10^{-5}$	42	1
3-hydroxyacyl-CoA dehydrogenase type-2	HCD2_HUMAN	1.00	2.60	2.6	1.01	2.00	2.0	2.05	1.46	-1.4	$7.43x10^{-4}$	109	2
40S ribosomal protein S24	RS24_HUMAN	1.00	1.61	1.6	1.30	1.64	1.3	1.57	1.44	-1.1	$3.35x10^{-4}$	78	1
40S ribosomal protein S4, X isoform	RS4X_HUMAN	1.00	1.95	1.9	1.51	1.79	1.2	1.71	1.31	-1.3	$9.53x10^{-8}$	181	3
40S ribosomal protein S7	RS7_HUMAN	1.26	1.47	1.2	1.25	1.43	1.1	1.67	1.00	-1.7	$4.47x10^{-2}$	197	3
40S ribosomal protein SA	RSSA_HUMAN	1.00	2.54	2.5	2.08	1.72	-1.2	1.89	1.89	1.0	$7.79x10^{-6}$	49	1
4-aminobutyrate aminotransferase, mitochondrial	GABT_HUMAN	3.56	2.65	-1.3	1.00	1.63	1.6	2.62	1.84	-1.4	$1.05x10^{-2}$	148	2
60 kDa heat shock protein, mitochondrial	CH60_HUMAN	1.89	3.23	1.7	1.00	2.65	2.6	2.12	1.32	-1.6	$1.71x10^{-9}$	1,439	18
60S ribosomal protein L5	RL5_HUMAN	1.13	2.26	2.0	1.00	1.38	1.4	1.86	1.34	-1.4	$6.69x10^{-5}$	103	1
60S ribosomal protein L6	RL6_HUMAN	1.00	1.65	1.7	2.34	1.97	-1.2	2.05	2.02	1.0	$3.02x10^{-3}$	220	3
60S ribosomal protein L8	RL8_HUMAN	1.27	1.60	1.3	1.65	1.77	1.1	1.87	1.00	-1.9	$5.90x10^{-3}$	62	1
6-phosphogluconate dehydrogenase, decarboxylating	6PGD_HUMAN	1.65	1.50	-1.1	1.80	1.64	-1.1	1.57	1.00	-1.6	$7.27x10^{-4}$	138	3
Acetyl-CoA acetyltransferase, mitochondrial	THIL_HUMAN	1.21	1.62	1.3	1.00	1.58	1.6	1.77	1.15	-1.5	$2.29x10^{-2}$	84	1
Actin, alpha cardiac muscle 1	ACTC_HUMAN	1.00	5.92	5.9	1.88	2.57	1.4	2.59	2.60	1.0	$1.11x10^{-11}$	711	9
Actin, cytoplasmic 1	ACTB_HUMAN	1.00	4.89	4.9	1.44	1.99	1.4	2.09	2.30	1.1	$1.76x10^{-5}$	1,290	15
Actin-related protein 3	ARP3_HUMAN	2.43	2.74	1.1	1.04	1.52	1.5	2.92	1.00	-2.9	$1.02x10^{-3}$	62	1
Adenine phosphoribosyltransferase	APT_HUMAN	1.50	2.62	1.7	1.00	2.33	2.3	2.10	1.14	-1.8	$9.79x10^{-6}$	266	3
Adenylate kinase 2, mitochondrial	KAD2_HUMAN	4.10	4.20	1.0	1.00	2.64	2.6	5.79	2.22	-2.6	$1.27x10^{-5}$	36	1
Adenylyl cyclase-associated protein 1	CAP1_HUMAN	3.30	4.26	1.3	1.96	3.87	2.0	4.73	1.00	-4.7	$2.97x10^{-4}$	61	1
Alanine-tRNA ligase, cytoplasmic	SYAC_HUMAN	1.33	1.82	1.4	1.29	1.83	1.4	2.31	1.00	-2.3	$3.69x10^{-5}$	263	4
Alpha-enolase	ENOA_HUMAN	1.00	1.78	1.8	1.28	1.51	1.2	1.33	1.20	-1.1	$4.48x10^{-10}$	1,225	13
Annexin A5	ANXA5_HUMAN	1.14	1.53	1.3	1.31	1.60	1.2	1.53	1.00	-1.5	$4.14x10^{-3}$	228	3
Aspartate aminotransferase, mitochondrial	AATM_HUMAN	1.00	1.80	1.8	1.63	1.56	1.0	1.55	2.64	1.7	$1.56x10^{-7}$	137	2
ATP synthase F(0) complex subunit B1, mitochondrial	AT5F1_HUMAN	2.52	4.08	1.6	1.00	2.42	2.4	3.86	1.42	-2.7	$2.23x10^{-5}$	44	1
ATP-citrate synthase	ACLY_HUMAN	2.07	3.19	1.5	1.00	3.28	3.3	2.75	2.15	-1.3	$5.46x10^{-3}$	110	2
ATP-dependent RNA helicase A	DHX9_HUMAN	2.33	3.73	1.6	1.00	2.29	2.3	3.09	1.73	-1.8	$3.24x10^{-3}$	356	5
ATP-dependent RNA helicase DDX1	DDX1_HUMAN	2.28	2.34	1.0	1.33	1.44	1.1	2.80	1.00	-2.8	$7.68x10^{-3}$	45	1
Barrier-to-autointegration factor	BAF_HUMAN	1.00	2.34	2.3	2.23	2.72	1.2	1.64	1.91	1.2	$1.90x10^{-2}$	78	1

Table I. Continued.

Protein name	Protein accession	Relative protein expression levels									ANOVA P-value	Protein score	Identified peptides
		Monolayer			Anoikis resistance			Reseeding					
Bifunctional glutamate/proline-RNA ligase	SYEP_HUMAN	1.23	1.22	1.0	1.00	1.42	1.4	1.71	1.03	-1.7	$3.87x10^{-4}$	146	3
Bifunctional purine biosynthesis protein PURH	PUR9_HUMAN	1.00	1.53	1.5	1.70	1.56	-1.1	1.41	1.75	1.2	$3.82x10^{-5}$	43	1
C-1-tetrahydrofolate synthase, cytoplasmic	C1TC_HUMAN	1.00	1.23	1.2	1.16	1.56	1.3	1.54	1.00	-1.5	$1.31x10^{-5}$	163	4
Calmodulin	CALM_HUMAN	1.00	1.59	1.6	2.11	1.77	-1.2	1.60	1.63	1.0	$1.36x10^{-4}$	43	1
Calreticulin	CALX_HUMAN	1.00	1.56	1.6	1.63	1.57	1.0	1.73	2.16	1.3	$1.66x10^{-7}$	208	3
Catechol O-methyltransferase	COMT_HUMAN	1.00	1.57	1.6	1.17	2.07	1.8	1.23	2.58	2.1	$8.50x10^{-4}$	138	2
Cathepsin D	CATD_HUMAN	1.00	1.60	1.6	1.28	1.16	-1.1	1.24	1.44	1.2	$3.04x10^{-6}$	283	5
Cell division control protein 42 homolog	CDC42_HUMAN	1.00	1.20	1.2	1.09	1.30	1.2	1.18	2.09	1.8	$3.85x10^{-3}$	100	2
Chromobox protein homolog 3	CBX3_HUMAN	1.68	1.45	-1.2	2.20	1.28	-1.7	1.40	1.00	-1.4	$6.12x10^{-3}$	98	2
Coatomer subunit gamma-1	COPG1_HUMAN	1.89	2.24	1.2	1.00	1.94	1.9	2.37	1.48	-1.6	$1.91x10^{-3}$	185	3
Costars family protein ABRACL	ABRAL_HUMAN	1.30	2.00	1.5	1.08	1.91	1.8	1.72	1.00	-1.7	$8.85x10^{-3}$	65	1
CTP synthase 1	PYRG1_HUMAN	2.17	2.29	1.1	1.00	2.54	2.5	2.64	1.68	-1.6	$4.27x10^{-3}$	60	1
Cullin-associated NEDD8-dissociated protein 1	CAND1_HUMAN	1.31	1.66	1.3	1.06	1.63	1.5	2.27	1.00	-2.3	$1.48x10^{-3}$	207	4
Deoxynucleoside triphosphate triphosphohydrolase SAMHD1	SAMH1_HUMAN	8.52	11.90	1.4	1.00	6.12	6.1	14.69	5.63	-2.6	$1.34x10^{-6}$	41	1
Destrin	DEST_HUMAN	1.00	1.71	1.7	1.13	2.01	1.8	1.36	1.31	1.0	$4.67x10^{-5}$	171	3
DNA mismatch repair protein Msh6	MSH6_HUMAN	2.87	1.71	-1.7	1.00	1.80	1.8	1.96	1.92	1.0	$1.10x10^{-3}$	41	1
DNA-dependent protein kinase catalytic subunit	PRKDC_HUMAN	3.31	3.26	1.0	1.00	1.59	1.6	2.28	1.54	-1.5	$2.52x10^{-3}$	212	5
Dolichyl-diphosphooligosaccharide-protein glycosyltransferase subunit 2	RPN2_HUMAN	1.37	1.64	1.2	1.00	1.79	1.8	1.70	1.76	1.0	$1.12x10^{-3}$	71	1
E3 ubiquitin/ISG15 ligase TRIM25	TRI25_HUMAN	2.83	2.91	1.0	1.00	2.37	2.4	3.70	1.28	-2.9	$1.39x10^{-7}$	62	1
eIF-2-alpha kinase activator GCN1	GCN1_HUMAN	3.37	3.90	1.2	1.00	4.02	4.0	4.42	1.92	-2.3	$1.17x10^{-4}$	109	3
Electron transfer flavoprotein subunit alpha, mitochondrial	ETFA_HUMAN	2.32	2.75	1.2	1.00	2.18	2.2	3.72	1.41	-2.6	$1.93x10^{-3}$	237	4
Elongation factor 1-alpha 1	EF1A1_HUMAN	1.00	1.70	1.7	1.67	1.61	1.0	1.52	1.08	-1.4	$1.18x10^{-8}$	1,010	13
Elongation factor 2	EF2_HUMAN	1.24	2.26	1.8	1.22	1.90	1.6	1.93	1.00	-1.9	$1.80x10^{-9}$	1,447	23
Epiplakin	EPIPL_HUMAN	1.87	2.56	1.4	1.00	1.67	1.7	2.78	1.41	-2.0	$4.01x10^{-4}$	444	9
Ezrin	EZRI_HUMAN	2.21	2.88	1.3	1.00	1.77	1.8	3.38	1.27	-2.7	$5.41x10^{-3}$	283	4
Eukaryotic initiation factor 4A-I	IF4A1_HUMAN	1.40	2.36	1.7	1.00	1.83	1.8	1.80	1.06	-1.7	$2.85x10^{-4}$	148	2
Eukaryotic translation initiation factor 1	EIF1_HUMAN	1.20	1.72	1.4	1.00	1.67	1.7	1.84	1.19	-1.5	$1.48x10^{-3}$	90	1
Eukaryotic translation initiation factor 3 subunit E	EIF3E_HUMAN	2.79	3.25	1.2	1.00	2.61	2.6	3.05	1.38	-2.2	$3.06x10^{-5}$	44	1
Eukaryotic translation initiation factor 3 subunit F	EIF3F_HUMAN	2.29	3.32	1.5	1.00	2.82	2.8	2.91	1.07	-2.7	$3.97x10^{-3}$	122	1
Eukaryotic translation initiation factor 3 subunit K	EIF3K_HUMAN	2.50	4.31	1.7	1.00	3.23	3.2	4.43	2.45	-1.8	$1.05x10^{-6}$	48	1

Table I. Continued.

Protein name	Protein accession	Relative protein expression levels									ANOVA P-value	Protein score	Identified peptides
		Monolayer			Anoikis resistance			Reseeding					
Eukaryotic translation initiation factor 4 gamma 1	IF4G1_HUMAN	1.00	2.09	2.1	1.18	2.19	1.9	1.78	1.34	-1.3	$1.84x10^{-3}$	129	3
Eukaryotic translation initiation factor 5A-1	IF5A1_HUMAN	1.12	2.32	2.1	1.51	1.94	1.3	1.69	1.00	-1.7	$1.85x10^{-4}$	240	4
Exportin-2	XPO2_HUMAN	1.80	2.06	1.1	1.00	1.79	1.8	1.90	1.01	-1.9	$1.60x10^{-3}$	111	2
Fatty acid synthase	FAS_HUMAN	1.96	2.39	1.2	1.89	2.50	1.3	2.57	1.00	-2.6	$2.03x10^{-7}$	1,031	16
Fructose-bisphosphate aldolase A	ALDOA_HUMAN	1.00	1.52	1.5	1.78	1.62	-1.1	1.30	1.58	1.2	$3.38x10^{-8}$	1,003	16
Glucosamine 6-phosphate N-acetyltransferase	GNA1_HUMAN	1.00	1.75	1.7	1.55	1.66	1.1	1.40	1.85	1.3	$7.32x10^{-3}$	53	1
Glucose-6-phosphate isomerase	G6PI_HUMAN	1.06	2.04	1.9	1.21	1.55	1.3	1.51	1.00	-1.5	$4.33x10^{-5}$	400	4
Glucosidase 2 subunit beta	GLU2B_HUMAN	1.73	1.20	-1.4	1.35	1.00	-1.4	1.35	2.08	1.5	$1.70x10^{-3}$	51	1
Glutaredoxin-3	GLRX3_HUMAN	1.00	1.51	1.5	1.08	1.53	1.4	1.40	1.33	-1.1	$1.16x10^{-3}$	46	1
Glutathione S-transferase Mu 3	GSTM3_HUMAN	1.30	1.58	1.2	1.35	1.80	1.3	1.60	1.00	-1.6	$3.53x10^{-4}$	213	4
Glyceraldehyde-3-phosphate dehydrogenase	G3P_HUMAN	1.00	3.15	3.1	1.64	2.02	1.2	1.81	1.46	-1.2	$4.81x10^{-10}$	771	7
Glycine--tRNA ligase	SYG_HUMAN	1.10	1.42	1.3	1.20	1.23	1.0	1.55	1.00	-1.6	$1.08x10^{-3}$	48	1
GMP synthase [glutamine-hydrolyzing]	GUAA_HUMAN	1.00	1.11	1.1	1.07	1.51	1.4	1.80	1.13	-1.6	$2.83x10^{-3}$	45	1
GTP-binding nuclear protein Ran	RAN_HUMAN	1.00	1.67	1.7	1.88	1.89	1.0	1.50	1.66	1.1	$1.57x10^{-3}$	57	1
Heat shock factor-binding protein 1	HSBP1_HUMAN	3.19	6.79	2.1	1.00	3.58	3.6	4.54	1.48	-3.1	$1.07x10^{-6}$	59	1
Heat shock protein beta-1	HSPB1_HUMAN	1.00	1.83	1.8	1.81	2.18	1.2	1.52	2.51	1.6	$1.82x10^{-10}$	370	6
Heat shock protein HSP 90-alpha	HS90A_HUMAN	1.00	1.85	1.9	1.42	1.63	1.1	1.32	1.25	-1.1	$2.10x10^{-9}$	1,505	22
Heterogeneous nuclear ribonucleoproteins C1/C2	HNRPC_HUMAN	1.00	1.55	1.5	1.72	1.69	1.0	1.72	1.70	1.0	$3.08x10^{-9}$	249	3
Heterogeneous nuclear ribonucleoprotein H	HNRH1_HUMAN	1.00	1.77	1.8	1.84	1.60	-1.2	1.79	1.93	1.1	$7.75x10^{-6}$	195	3
Heterogeneous nuclear ribonucleoprotein K	HNRPK_HUMAN	1.48	1.44	1.0	1.17	1.39	1.2	1.83	1.00	-1.8	$3.86x10^{-5}$	454	6
Histone H2A type 1-A	H2A1A_HUMAN	1.79	1.76	1.0	1.29	1.79	1.4	2.49	1.00	-2.5	$1.36x10^{-3}$	272	3
Histone H2A type 1-D	H2A1D_HUMAN	1.24	1.26	1.0	1.85	1.42	-1.3	2.12	1.00	-2.1	$1.05x10^{-3}$	285	3
Histone H2B type F-S	H2BFS_HUMAN	1.00	3.42	3.4	1.29	1.49	1.2	1.81	1.07	-1.7	$1.20x10^{-6}$	305	5
Histone H3	H3_HUMAN	1.52	1.23	-1.2	1.94	1.35	-1.4	1.78	1.00	-1.8	$7.41x10^{-7}$	226	12
Histone H4	H4_HUMAN	1.00	1.22	1.2	1.42	1.16	-1.2	1.53	1.02	-1.5	$6.19x10^{-8}$	473	6
Hydroxyacyl-coenzyme A dehydrogenase, mitochondrial	HCDH_HUMAN	4.44	5.04	1.1	1.00	2.45	2.4	5.43	1.10	-4.9	$1.09x10^{-3}$	175.8	1
Hypoxanthine-guanine phosphoribosyltransferase	HPRT_HUMAN	1.00	1.20	1.2	1.56	1.39	-1.1	1.31	1.68	1.3	$5.20x10^{-5}$	70.8	3
Importin-4	IPO4_HUMAN	1.30	1.00	-1.3	1.99	1.29	-1.5	1.72	1.27	-1.4	$7.64x10^{-4}$	98	2
Importin subunit beta-1	IMB1_HUMAN	1.72	2.49	1.4	1.50	2.04	1.4	2.65	1.00	-2.7	$1.35x10^{-3}$	40	3
Inorganic pyrophosphatase	IPYR_HUMAN	1.00	2.48	2.5	1.46	2.21	1.5	1.94	1.47	-1.3	$2.62x10^{-4}$	106	2
Insulin receptor substrate 4	IRS4_HUMAN	1.00	1.85	1.8	2.49	2.91	1.2	1.76	5.76	3.3	$1.11x10^{-11}$	41	1

Table I. Continued.

Protein name	Protein accession	Relative protein expression levels									ANOVA P-value	Protein score	Identified peptides
		Monolayer			Anoikis resistance			Reseeding					
Interferon-induced, double-stranded RNA-activated protein kinase	E2AK2_HUMAN	1.56	1.39	-1.1	1.03	1.48	1.4	1.63	1.00	-1.6	$2.64x10^{-3}$	52	1
Isocitrate dehydrogenase [NADP], mitochondrial	IDHC_HUMAN	1.00	1.37	1.4	1.50	1.40	-1.1	1.52	2.46	1.6	$4.05x10^{-10}$	851	3
Keratin, type I cytoskeletal 16	K1C16_HUMAN	1.00	1.46	1.5	1.58	1.38	-1.2	1.50	4.81	3.2	$9.90x10^{-8}$	483	8
Keratin, type I cytoskeletal 18	K1C18_HUMAN	1.68	3.65	2.2	1.00	2.15	2.1	3.47	1.94	-1.8	$2.95x10^{-9}$	1,518	20
Keratin, type I cytoskeletal 19	K1C19_HUMAN	1.48	1.94	1.3	1.00	1.67	1.7	2.11	1.39	-1.5	$1.34x10^{-5}$	1,250	18
Keratin, type I cytoskeletal 9	K1C9_HUMAN	1.27	1.00	-1.3	1.33	1.07	-1.3	1.15	4.79	4.2	$1.41x10^{-9}$	388	3
Keratin, type II cytoskeletal 1	K2C1_HUMAN	1.00	1.06	1.1	1.25	1.18	-1.1	1.07	3.17	3.0	$3.37x10^{-11}$	1,031	14
Keratin, type II cytoskeletal 8	K2C8_HUMAN	1.00	1.90	1.9	1.10	1.16	1.1	1.83	1.92	1.0	$3.85x10^{-13}$	2,284	28
Lactoylglutathione lyase	LGUL_HUMAN	1.30	2.13	1.6	1.26	2.41	1.9	1.86	1.00	-1.9	$7.22x10^{-3}$	65	1
Leucine-rich PPR motif-containing protein, mitochondrial	LPPRC_HUMAN	1.98	3.96	2.0	1.00	2.75	2.7	2.69	1.47	-1.8	$6.38x10^{-3}$	339	6
L-lactate dehydrogenase A chain	LDHA_HUMAN	1.00	2.73	2.7	1.38	1.73	1.3	1.44	1.18	-1.2	$5.11x10^{-9}$	684	10
Matrin-3	MATR3_HUMAN	1.32	1.70	1.3	1.17	1.60	1.4	2.11	1.00	-2.1	$1.85x10^{-3}$	85	2
Mitochondrial carrier homolog 2	MTCH2_HUMAN	2.45	3.09	1.3	1.00	1.77	1.8	2.96	1.55	-1.9	$2.27x10^{-3}$	42	1
NADP-dependent malic enzyme	MAOX_HUMAN	3.16	4.83	1.5	1.00	2.20	2.2	2.33	1.54	-1.5	$6.65x10^{-4}$	133	3
Neutral alpha-glucosidase AB	GANAB_HUMAN	1.47	1.18	-1.2	1.61	1.00	-1.6	1.51	1.58	1.0	$2.56x10^{-3}$	130	1
Nucleolar and coiled-body phosphoprotein 1	NOLC1_HUMAN	2.25	2.70	1.2	1.00	1.91	1.9	3.49	1.21	-2.9	$1.70x10^{-5}$	255	1
Nucleolar protein 58	NOP58_HUMAN	1.66	2.93	1.8	1.00	2.47	2.5	2.66	1.95	-1.4	$1.69x10^{-3}$	56	1
Nucleophosmin	NPM_HUMAN	1.01	1.20	1.2	1.19	1.12	-1.1	1.70	1.00	-1.7	$3.97x10^{-5}$	450	4
Nucleoside diphosphate kinase A	NP1L1_HUMAN	1.00	2.18	2.2	1.68	1.58	-1.1	1.78	1.44	-1.2	$8.69x10^{-5}$	313	2
PCTP-like protein	PCTL_HUMAN	1.00	1.89	1.9	1.53	1.97	1.3	1.55	1.85	1.2	$7.96x10^{-11}$	48	6
Peptidyl-prolyl cis-trans isomerase A	PPIA_HUMAN	1.00	1.83	1.8	1.70	1.71	1.0	1.56	1.31	-1.2	$8.94x10^{-11}$	321	5
Peptidyl-prolyl cis-trans isomerase FKBP4	FKBP4_HUMAN	1.00	1.99	2.0	1.95	1.78	-1.1	1.86	2.05	1.1	$3.23x10^{-5}$	218	10
Peroxiredoxin-5, mitochondrial	PRDX5_HUMAN	1.07	2.04	1.9	1.00	1.79	1.8	1.91	1.45	-1.3	$1.29x10^{-3}$	240	2
Phosphatidylethanolamine-binding protein 1	PEBP1_HUMAN	1.00	1.54	1.5	1.96	1.78	-1.1	1.36	1.72	1.3	$3.38x10^{-7}$	49	4
Pirin	PIR_HUMAN	2.58	2.46	-1.1	1.00	2.30	2.3	2.38	1.44	-1.7	$4.75x10^{-5}$	34	1
Plasminogen activator inhibitor 1 RNA-binding protein	PAIRB_HUMAN	2.27	1.37	-1.7	1.70	1.21	-1.4	1.09	1.00	-1.1	$7.51x10^{-3}$	42	3
Plastin-3	PLST_HUMAN	2.17	2.65	1.2	1.00	2.76	2.8	2.80	1.71	-1.6	$5.86x10^{-4}$	270	2
Polypyrimidine tract-binding protein 1	PTBP1_HUMAN	1.40	2.63	1.9	1.02	1.86	1.8	2.11	1.00	-2.1	$6.25x10^{-5}$	142	4

Table I. Continued.

Protein name	Protein accession	Relative protein expression levels									ANOVA P-value	Protein score	Identified peptides
		Monolayer			Anoikis resistance			Reseeding					
Profilin-1	PROF1_HUMAN	1.00	1.50	1.5	1.84	1.69	-1.1	1.48	1.67	1.1	$2.68x10^{-5}$	70	1
Prostaglandin E synthase 3	TEBP_HUMAN	1.00	1.66	1.7	1.48	1.99	1.3	1.60	1.48	-1.1	$4.15x10^{-6}$	130	1
Proteasome activator complex subunit 2	PSME2_HUMAN	1.39	1.64	1.2	1.06	1.71	1.6	2.94	1.00	-2.9	$4.14x10^{-3}$	41	4
Proteasome subunit beta type-1	PSB1_HUMAN	4.02	6.17	1.5	1.00	1.57	1.6	2.54	2.57	1.0	$2.00x10^{-3}$	43	1
Protein disulfide-isomerase	PDIA1_HUMAN	1.00	1.52	1.5	1.61	1.47	-1.1	1.76	2.00	1.1	$9.31x10^{-4}$	334	4
Protein dpy-30 homolog	DPY30_HUMAN	2.72	4.32	1.6	1.33	1.95	1.5	2.66	1.00	-2.7	$3.92x10^{-3}$	160	1
Protein phosphatase 1 regulatory subunit 14B	PP14B_HUMAN	3.32	4.94	1.5	1.00	2.22	2.2	2.54	1.63	-1.6	$6.38x10^{-5}$	67	1
Protein phosphatase 1 regulatory subunit 7	PP1R7_HUMAN	2.03	2.87	1.4	1.00	2.70	2.7	2.99	1.39	-2.1	$1.92x10^{-4}$	47	1
Protein S100-A11	S10AB_HUMAN	1.00	2.58	2.6	1.76	2.19	1.2	2.24	1.64	-1.4	$9.21x10^{-7}$	60	4
Protein unc-45 homolog A	UN45A_HUMAN	4.98	4.88	1.0	1.00	2.03	2.0	3.41	2.44	-1.4	$7.43x10^{-5}$	200	1
Prothymosin alpha	PTMA_HUMAN	1.24	1.00	-1.2	1.81	1.03	-1.8	1.47	1.32	-1.1	$2.79x10^{-3}$	113	2
Pyruvate kinase PKM	KPYM_HUMAN	1.00	1.88	1.9	1.46	1.71	1.2	1.45	1.41	1.0	$2.51x10^{-11}$	111	24
Rab GDP dissociation inhibitor beta	GDIB_HUMAN	1.10	2.34	2.1	1.09	1.62	1.5	1.73	1.00	-1.7	$2.92x10^{-6}$	1,781	4
Ras-related protein Rab-7a	RAB7A_HUMAN	1.00	1.84	1.8	1.45	1.64	1.1	1.59	2.00	1.3	$2.99x10^{-3}$	46	2
Ribosomal L1 domain-containing protein 1	RL1D1_HUMAN	1.11	1.58	1.4	1.00	1.44	1.4	1.93	1.25	-1.5	$6.82x10^{-3}$	151	2
Small nuclear ribonucleoprotein Sm D1	SMD1_HUMAN	7.94	8.86	1.1	2.45	4.59	1.9	8.44	1.00	-8.4	$6.44x10^{-8}$	57	1
Serine hydroxymethyltransferase, mitochondrial	GLYM_HUMAN	1.00	1.60	1.6	1.68	1.66	-1.0	1.53	1.36	-1.1	$2.48x10^{-4}$	31	1
Serine/arginine-rich splicing factor 7	SRSF7_HUMAN	1.00	1.39	1.4	1.43	1.89	1.3	1.81	2.76	1.5	$8.72x10^{-4}$	67	1
Serine/threonine-protein phosphatase 2A 65 kDa regulatory subunit A alpha isoform	2AAA_HUMAN	1.00	1.59	1.6	1.54	1.51	1.0	1.53	1.75	1.1	$8.57x10^{-3}$	290	6
Serine/threonine-protein phosphatase PP1-beta catalytic subunit	PP1B_HUMAN	1.14	1.53	1.3	1.04	1.48	1.4	1.57	1.00	-1.6	$1.09x10^{-8}$	187	3
Serpin H1	SERPH_HUMAN	1.28	1.41	1.1	1.00	1.37	1.4	1.66	1.10	-1.5	$6.96x10^{-9}$	290	4
Serum albumin	ALBU_HUMAN	1.11	1.90	1.7	1.00	1.28	1.3	1.53	1.08	-1.4	$1.26x10^{-3}$	37	2
Single-stranded DNA-binding protein, mitochondrial	SSBP_HUMAN	1.00	1.38	1.4	1.06	1.21	1.1	1.46	2.24	1.5	$2.48x10^{-4}$	69	2
S-formylglutathione hydrolase	ESTD_HUMAN	1.00	1.34	1.3	1.60	1.79	1.1	1.19	2.89	2.4	$2.74x10^{-7}$	111	1
Succinate dehydrogenase [ubiquinone] flavoprotein subunit, mitochondrial	SDHA_HUMAN	2.11	2.55	1.2	1.00	2.55	2.5	2.67	1.85	-1.4	$1.34x10^{-3}$	66	1
T-complex protein 1 subunit epsilon	TCPE_HUMAN	1.41	1.75	1.2	1.15	1.58	1.4	1.90	1.00	-1.9	$1.88x10^{-3}$	207	3
T-complex protein 1 subunit eta	TCPH_HUMAN	1.05	1.51	1.4	1.00	1.52	1.5	1.34	1.00	-1.3	$6.04x10^{-3}$	232	3
T-complex protein 1 subunit zeta	TCPZ_HUMAN	2.44	2.98	1.2	1.30	2.31	1.8	2.89	1.00	-2.9	$4.95x10^{-5}$	98	2
Transgelin-2	TAGL2_HUMAN	1.21	1.46	1.2	1.39	1.63	1.2	1.67	1.00	-1.7	$3.13x10^{-3}$	167	4

Table I. Continued.

Protein name	Protein accession	Relative protein expression levels									ANOVA P-value	Protein score	Identified peptides
		Monolayer			Anoikis resistance			Reseeding					
Transketolase	TKT_HUMAN	1.00	1.64	1.6	1.33	1.52	1.1	1.42	1.01	-1.4	$4.56x10^{-8}$	333	7
tRNA (adenine(58)-N(1))-methyltransferase catalytic subunit TRMT61A	TRM61_HUMAN	1.00	1.47	1.5	1.99	1.69	-1.2	1.70	1.11	-1.5	$2.80x10^{-6}$	725	1
Tubulin alpha-1B chain	TBA1B_HUMAN	1.12	1.31	1.2	1.35	1.46	1.1	1.66	1.00	-1.7	$3.73x10^{-3}$	873	12
Tubulin beta chain	TBB5_HUMAN	1.00	1.80	1.8	1.71	1.90	1.1	1.70	1.36	-1.3	$1.00x10^{-4}$	999	16
U5 small nuclear ribonucleoprotein 200 kDa helicase	U520_HUMAN	1.73	1.93	1.1	1.00	1.69	1.7	2.17	1.26	-1.7	$6.34x10^{-3}$	265	1
Ubiquitin-like modifier-activating enzyme 1	UBA1_HUMAN	1.06	1.77	1.7	1.00	1.50	1.5	1.39	1.03	-1.3	$1.26x10^{-6}$	50	6
UDP-glucose 6-dehydrogenase	UGDH_HUMAN	1.67	1.99	1.2	1.00	2.00	2.0	1.72	1.13	-1.5	$1.69x10^{-3}$	341	2
UMP-CMP kinase	KCY_HUMAN	3.36	3.42	1.0	1.00	3.09	3.1	3.57	2.38	-1.5	$1.18x10^{-3}$	97	1
Uncharacterized protein C8orf48	CH048_HUMAN	2.33	2.15	-1.1	1.00	2.60	2.6	3.01	1.26	-2.4	$4.13x10^{-4}$	45	1
Vinculin	VINC_HUMAN	2.67	2.96	1.1	1.50	2.09	1.4	3.62	1.00	-3.6	$5.01x10^{-3}$	88	2
WD repeat-containing protein 61	WDR61_HUMAN	2.94	5.61	1.9	1.00	2.37	2.4	3.42	1.60	-2.1	$9.95x10^{-3}$	42	1
X-ray repair cross-complementing protein 5	XRCC5_HUMAN	2.22	2.73	1.2	1.00	2.10	2.1	1.76	1.22	-1.4	$6.63x10^{-3}$	44	2
X-ray repair cross-complementing protein 6	XRCC6_HUMAN	1.85	2.27	1.2	1.00	2.36	2.4	2.94	1.22	-2.4	$1.10x10^{-3}$	133	2

Protein expression levels defined as either; +, siOGT expression level > siSC or -, siSC expresison level > siOGT. P-values were calculated using Progenesis QI and the ANOVA test followed by Bonferroni's multiple comparison test. Protein scores were derived from the scores of all peptides identified using the Mascot search engine. $P \leq 0.01$ indicate a statistically significant difference. si, small interfering; OGT, *O*-GlcNAc transferase; SC, scramble control.

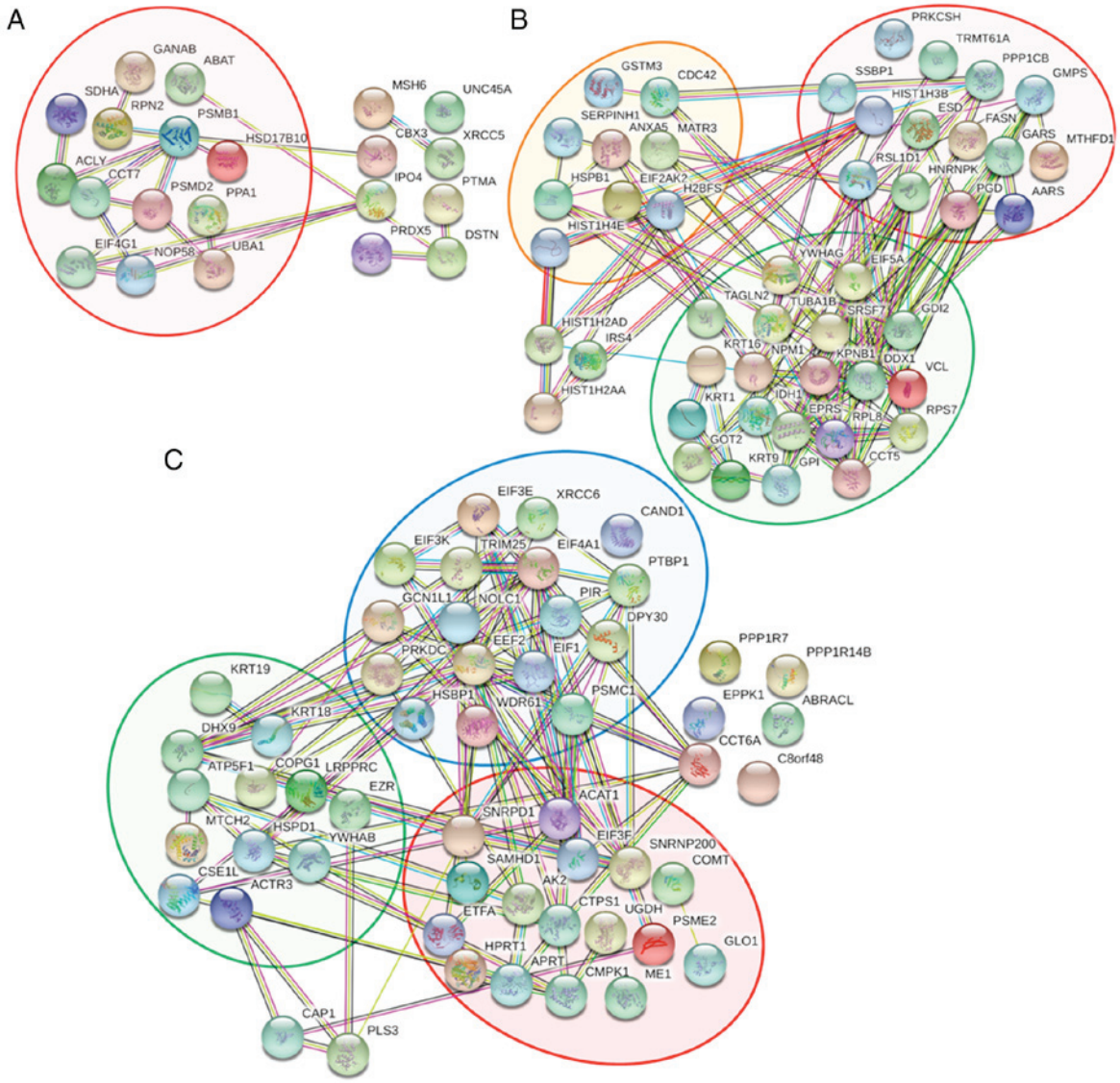

Figure 4. STRING analysis of protein-protein interaction networks present in the different culture conditions. STRING analysis of differentially expressed proteins affected by siOGT transfection in (A) anoikis resistant, (B) reseeding and (C) shared common in both anoikis resistant and reseeding conditions are presented. The interaction networks are clustered into different major groups including proteins associated with cellular metabolism (red background), cellular localization (green background), stress response (orange background) and gene expression regulation (blue background). STRING, Search Tool for the Retrieval of Interacting Genes/Proteins; OGT, *O*-GlcNAc transferase; si, small interfering.

differential expression between siSC and siOGT treated cells under anoikis resistant and reseeding conditions, representative proteins from each group were selected for validation using western blot analysis. The assessed proteins included proteins involved in cellular metabolism (histone H3 and SNRPD1), cellular localization (NMP1 and CK18) and stress response (HSP27) (Fig. 5A). The results from western blotting showed that expression of the proteins associated with cellular metabolism and localization (SNRPD1, histone H3, NMP1 and CK18) were significantly decreased following OGT knockdown compared with the siSC in the reseeding condition, however, expression of HSP27, a protein associated with the stress response, was increased following OGT silencing.

Furthermore, the expression levels of each protein identified using label-free quantitative proteomics and western blot analysis were compared and the trends of protein expressions are presented. The results demonstrated that in the anoikis-resistant condition, histone H3 and NMP1 were downregulated following OGT knockdown, whereas CK18, HSP27 and SNRPD1 were upregulated (Fig. 5B). In addition, under the reseeding conditions, the majority of the validated proteins including histone H3, SNRPD1, NMP1 and CK18 expression was downregulated following OGT silencing, whereas HSP27 expression was upregulated (Fig. 5C). Collectively, the protein expression patterns of all validated proteins obtained from the label-free and western blot analysis identified similar changes in protein expression.

Knockdown of O-GlcNAcylation and SNRPD1 expression results in downregulation of mTOR, particularly in the reseeding condition. Western blot analysis and label-free quantitative LC-MS revealed that the expression level of SNRPD1 was most significantly decreased following OGT knockdown

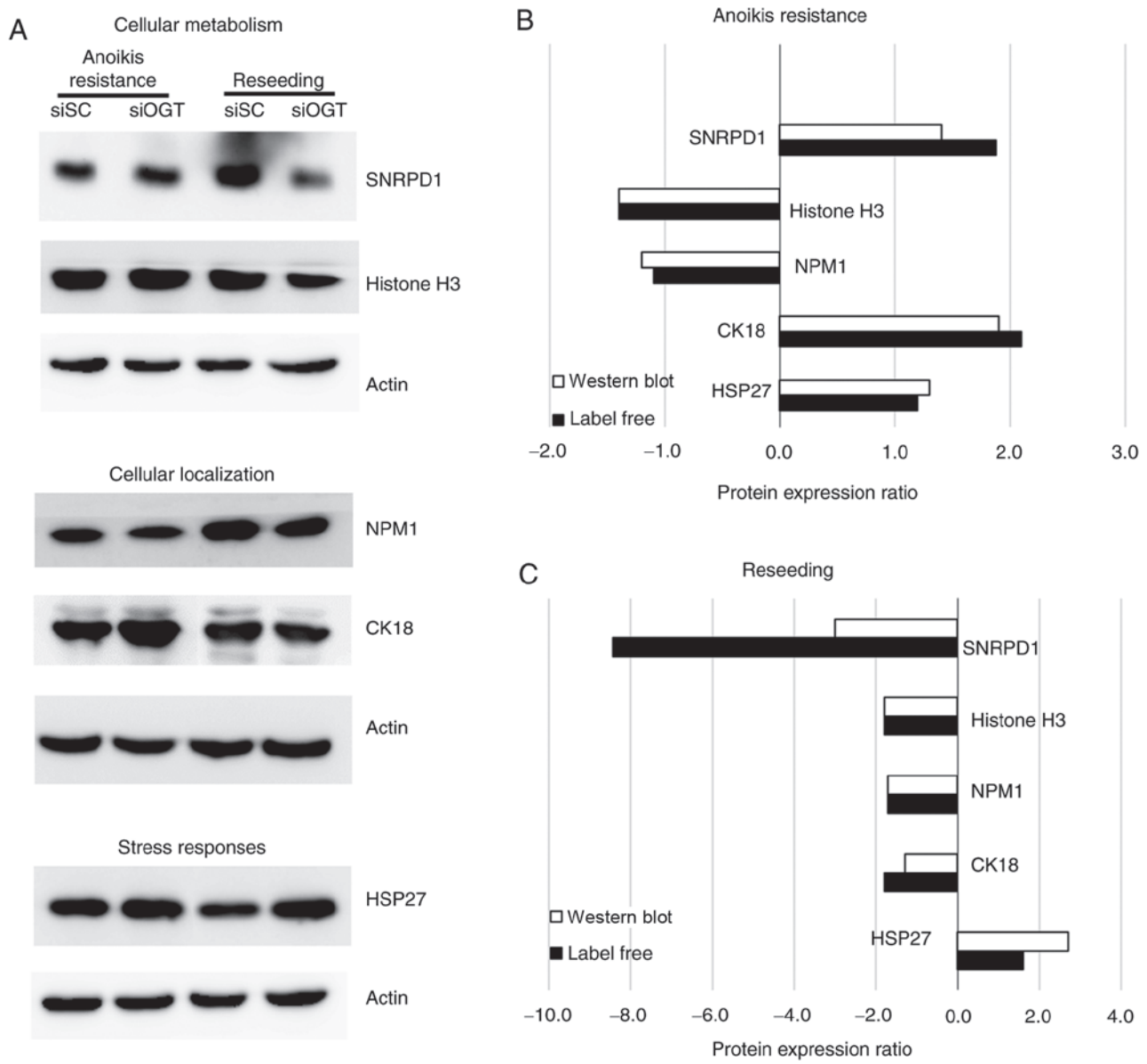

Figure 5. Validation and comparison of proteins analyzed by western blotting and label-free quantitative proteomics. (A) Representative western blots of proteins influencing cellular metabolism (SNRPD1 and Histone H3), cellular localization (NPM1 and CK18) and stress responses (HSP27) under anoikis resistant and reseeding conditions. β-actin bands corresponding to the same membranes were used as the loading control in all groups. Quantitative analysis of the expression ratio of the validated proteins between siSC and siOGT treated cells under (B) anoikis resistant and (C) reseeding conditions using western blotting (white bar) and label free quantitative proteomics (black bar). OGT, *O*-GlcNAc transferase; si, small interfering; HSP, heat shock protein; SNRPD1, small nuclear ribonucleoprotein Sm D1; NPM1, nucleophosmin; SNRPD1, small nuclear ribonucleoprotein Sm D1; CK18, type I cytoskeletal 18.

under the reseeding condition. Furthermore, a decrease in mTOR protein levels was observed in the SNRPD1 depleted cells ($P<0.01$; Fig. 6); suggesting an association between SNRPD1 and mTOR expression levels via *O*-GlcNAcylation reduction under the reseeding condition.

Discussion

Altered metabolism is one of the most important factors in the progression of various diseases, and particularly in cancer. The major characteristic of metabolic alteration in cancer cells is an increase in glucose consumption to facilitate rapid growth and cell proliferation (6). Fairly small amounts of glucose can enter the HBP, which is a minor branch of the glycolytic pathway. The HBP end product is UDP-GlcNAc, a sugar donor for post-translational protein modification of *O*-GlcNAcylation (7), and increasing evidence has suggested that aberrant *O*-GlcNAcylation is associated with malignant tumors (10,11). Therefore, in the present study, the effects of *O*-GlcNAc alteration on the malignant transformation of MCF-7 breast cancer cells were examined under different culture conditions used to mimic specific stages of the metastatic process. OGT silencing was used to reduce the levels of *O*-GlcNAcylated proteins in the cells. The current results revealed that efficient knockdown of OGT gene expression was achieved in all culture conditions, and that it resulted in notably altered cellular morphology in the reseeding condition only, where the cells resembled the morphology and growth of cancer cells at distant sites.

OGT is essential for cell viability and OGT depletion results in embryonic lethality (20). Moreover, our previous

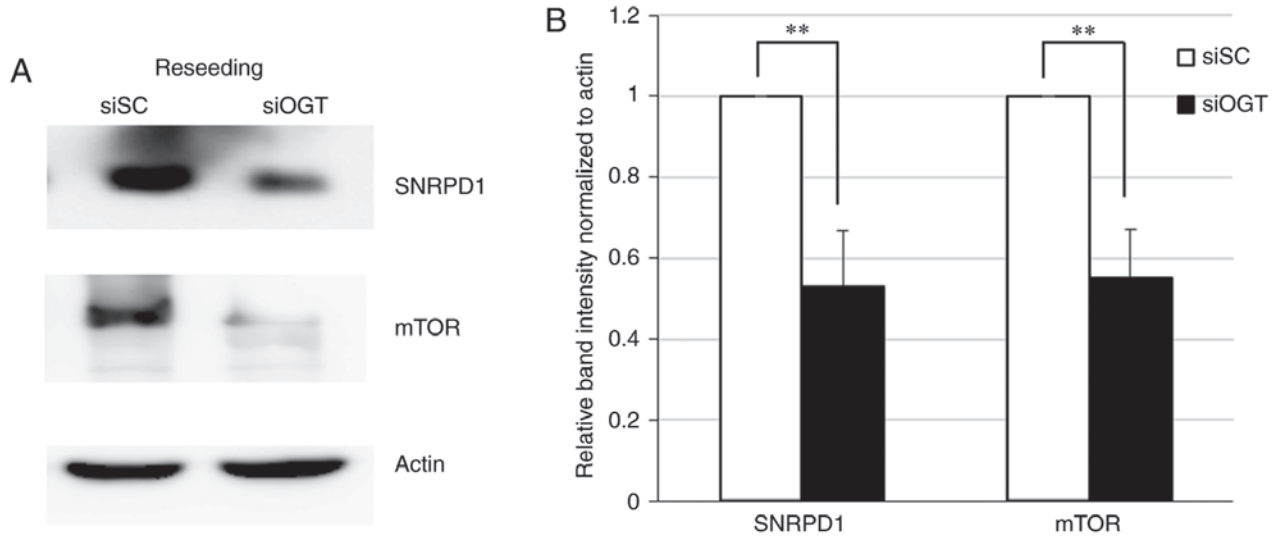

Figure 6. Changes in SNRPD1 and mTOR expression levels following OGT knockdown under the reseeding condition. (A) Representative western blots of SNRPD1, mTOR and β-actin. (B) densitometry analysis of SNRPD1 and mTOR, normalized to β-actin. **P<0.01 vs. siSC. SNRPD1, small nuclear ribonucleoprotein Sm D1; si, small interfering, OGT, *O*-GlcNAc transferase; SC, scramble control.

study revealed that OGT knockdown caused a marked decrease in cell viability under the anoikis resistant conditions (14). Furthermore, OGT silencing reduces the migratory and invasive capacities in a number of different types of cancer including breast (21), prostate (22), ovarian (23) and colon cancer (24). In the present study, it was revealed that, although OGT knockdown using RNA interference did not significantly influence cell growth and proliferation in the monolayer condition, it decreased the cell viability and invasiveness of MCF-7 cells under the anoikis resistant and reseeding culture conditions, which are hypothesized to be crucial steps in cancer metastasis (25,26).

Since siOGT treatment affected cell viability and invasive protrusion under the anoikis resistant and reseeding conditions, label-free quantitative proteomics and LC-MS/MS were used to determine protein expression changes affected by *O*-GlcNAc knockdown. The heat map data demonstrated significant alterations in the expression of 317 proteins affected by siOGT treatment in all culture conditions. Notably, *O*-GlcNAc reduction significantly resulted in downregulation of 85 proteins under the reseeding condition, which may be associated with the altered cell morphology and a decrease in cell viability and invasiveness. Therefore, this may suggest that in the reseeding condition used to mimic the growth and proliferation of metastatic cancer cells at secondary sites, *O*-GlcNAcylation may serve an important role in the metastatic cancer cascade of breast cancer. The differentially expressed proteins (>1.5 fold) were used to develop a protein-protein interaction network. STRING analysis of proteins expressed in the anoikis resistant and reseeding conditions revealed that the majority of differentially expressed proteins were involved in a number cellular processes, including cellular metabolism (SNRNPD1 and Histone H3), cellular localization (NPM1 and CK18) and the stress responses (HSP27).

Histone H3 is reported to be modified by *O*-GlcNAc, which regulates various biological processes in cells (27); moreover, decreasing expression of histone H3 by stable knockdown resulted in decreased neoplastic cell transformation (28). NPM1 is also an *O*-GlcNAcylated protein and its modification is associated with the progression of cholangiocarcinoma (29). Reducing NPM1 expression using siRNA resulted in a significant decrease in cell proliferation and induced cell cycle arrest in leukemia, colon and breast cancer (30-32). Moreover, the present study supports the results of previous studies which have demonstrated that *O*-GlcNAc regulates the cellular stress responses via the expression of numerous HSPs, including HSP27 (14,33). HSP27 expression levels affect cell proliferation, migration and invasion abilities in several types of cancer, such as liver, prostate and breast cancer (34-36).

Subsequently, representative proteins were selected for validation and the protein expression ratio (siSC vs. siOGT) from western blots and label-free quantitative analysis were analyzed. SNRPD1, Histone H3, NPM1 and CK18 expression was significantly downregulated, whereas HSP27 expression was upregulated following OGT knockdown. Hsp27 has been implicated in the stress response mechanism in cancer cells (14). Furthermore, Hsp27 exerts tumor suppressor functions to inhibit cancer progression and metastasis. As transient OGT knockdown resulted in a significant decrease in invasion, in the anoikis resistant and reseeding conditions; it is possible that a decrease in *O*-GlcNAcylation via OGT knockdown may increase cellular stress, resulting in the upregulation of Hsp27 which serves to limit and alleviate these conditions.

Changes in protein expression observed from immunoblots and label-free quantitative analysis revealed similar trends. OGT silencing in MCF-7 cells cultured under the reseeding condition revealed significant changes in the expression of certain proteins, which may influence cell viability and invasion (Fig. 2). This indicates that aberrant *O*-GlcNAcylation may serve a pivotal role under certain conditions to regulate the metastatic potential of malignant breast cancer cells.

Among the validated proteins, SNRPD1 exhibited the most significant decrease in expression levels following

OGT knockdown under the reseeding condition. Therefore, a focus was placed on this protein and its interacting partners. SNRPD1 serves a key role in pre-mRNA splicing (37) and exerts an inhibitory effect on cell growth and colony formation via cell cycle regulation in lung cancer (38). In addition, SNRPD1 depletion results in a notable loss of pluripotency and significantly prevents the reprogramming of human pluripotent stem cells (39). Moreover, gene microarray analysis demonstrated that SNRPD1 expression is upregulated in lung and breast cancer tissues (40). Furthermore, siRNA-mediated knockdown of SNRPD1 resulted in a marked reduction of cell viability and mTOR expression in malignant breast cancer cells (40). In the present study, MCF-7 cells transfected with siOGT exhibited significantly decreased SNRPD1 and mTOR expression levels, under the reseeding condition (Fig. 6). Notably, mTOR belongs to the serine/threonine protein kinase family and its signaling is usually activated in multiple types of cancer including breast cancer (41). Numerous studies have reported that activated mTOR signaling results in increased tumor progression and a decrease in patient survival (42-44). Furthermore, activation of the mTOR pathway promotes tumor growth and progression in 70% of all breast cancer cases (45). Therefore, blocking this pathway by inhibiting mTOR activation or decreasing its expression may serve as a promising strategy for cancer therapy. However, mTOR activation is dependent on various protein partners to form a complex, resulting in specific cellular signaling transduction (46-48). The present data revealed that OGT knockdown resulted in a decrease in mTOR protein expression level; however, the complexity of mTOR signalling means that further studies are needed to clarify which mTOR complex is implicated in OGT downregulation.

In conclusion, the results of the present study demonstrate the impact of a decrease *O*-GlcNAcylation on MCF-7 cells in terms of its biological effects as well as protein expression in *in vitro* models of primary, spheroid and secondary growth. Decreasing *O*-GlcNAcylation significantly altered cancer cell morphology, and reduced cell viability and invasiveness under the reseeding condition. Moreover, a number of proteins were downregulated following OGT knockdown under the reseeding condition, and these proteins may be potential candidates for targeted therapy. Notably, there was a significant decrease in SNRPD1 and mTOR expression levels following a decrease in *O*-GlcNAc in the reseeding condition. Therefore, the development of a novel strategy to inhibit SNRPD1 expression and downregulate the mTOR pathway may represent a novel therapeutic approach for treating patients with malignant breast cancer. Collectively, the current findings indicate that *O*-GlcNAcylation serves a pivotal role in specific steps of the metastatic processes in MCF-7 breast cancer cells.

Acknowledgements

Not applicable.

Funding

The research was supported by funding from the Chulabhorn Research Institute (grant no. BC-2008-02).

Availability of data and materials

The datasets used during the present study are available from the corresponding author upon reasonable request.

Authors' contributions

PN and VC conceived, designed the study, wrote and drafted the manuscript. PN performed the experiments in cell cultures, proteomics, immunoblotting and data analysis. DC prepared and ran samples for the LC-MS/MS. KS constructed and analyzed heat map data. CS interpreted the results and reviewed the manuscript. JS reviewed and edited the manuscript and was involved in the conception of the study. All authors read and approved the final version of the manuscript and agree to be accountable for all aspects of the research in ensuring that the accuracy or integrity of any part of the work are appropriately investigated and resolved.

Ethics approval and consent to participate

Not applicable.

Patient consent for publication

Not applicable.

Competing interests

The authors declare that they have no competing interests.

References

1. Bray F, Ferlay J, Soerjomataram I, Siegel RL, Torre LA and Jemal A: Global cancer statistics 2018: GLOBOCAN estimates of incidence and mortality worldwide for 36 cancers in 185 countries. CA Cancer J Clin 68: 394-424, 2018.
2. Caplan L: Delay in breast cancer: Implications for stage at diagnosis and survival. Front Public Health 2: 87, 2014.
3. Chaffer CL and Weinberg RA: A perspective on cancer cell metastasis. Science 331: 1559-1564, 2011.
4. Valastyan S and Weinberg RA: Tumor metastasis: Molecular insights and evolving paradigms. Cell 147: 275-292, 2011.
5. Redig AJ and McAllister SS: Breast cancer as a systemic disease: A view of metastasis. J Intern Med 274: 113-126, 2013.
6. Vander Heiden MG, Cantley LC and Thompson CB: Understanding the Warburg effect: The metabolic requirements of cell proliferation. Science 324: 1029-1033, 2009.
7. Hart GW, Housley MP and Slawson C: Cycling of O-linked beta-N-acetylglucosamine on nucleocytoplasmic proteins. Nature 446: 1017-1022, 2007.
8. Kreppel LK, Blomberg MA and Hart GW: Dynamic glycosylation of nuclear and cytosolic proteins. Cloning and characterization of a unique O-GlcNAc transferase with multiple tetratricopeptide repeats. J Biol Chem 272: 9308-9315, 1997.
9. Gao Y, Wells L, Comer FI, Parker GJ and Hart GW: Dynamic O-glycosylation of nuclear and cytosolic proteins: Cloning and characterization of a neutral, cytosolic beta-N-acetylglucosaminidase from human brain. J Biol Chem 276: 9838-9845, 2001.
10. Hanover JA, Chen W and Bond MR: O-GlcNAc in cancer: An Oncometabolism-fueled vicious cycle. J Bioenerg Biomembr 50: 155-173, 2018.
11. Chaiyawat P, Netsirisawan P, Svasti J and Champattanachai V: Aberrant O-GIcNAcylated proteins: New perspectives in breast and colorectal cancer. Front Endocrinol (Lausanne) 5: 193, 2014.
12. Champattanachai V, Netsirisawan P, Chaiyawat P, Phueaouan T, Charoenwattanasatien R, Chokchaichamnankit D, Punyarit P, Srisomsap C and Svasti J: Proteomic analysis and abrogated expression of O-GlcNAcylated proteins associated with primary breast cancer. Proteomics 13: 2088-2099, 2013.

13. PhueaouanT,ChaiyawatP,NetsirisawanP,ChokchaichamnankitD, Punyarit P, Srisomsap C, Svasti J and Champattanachai V: Aberrant O-GlcNAc-modified proteins expressed in primary colorectal cancer. Oncol Rep 30: 2929-2936, 2013.
14. Netsirisawan P, Chaiyawat P, Chokchaichamnankit D, Lirdprapamongkol K, Srisomsap C, Svasti J and Champattanachai V: Decreasing O-GlcNAcylation affects the malignant transformation of MCF-7 cells via Hsp27 expression and its O-GlcNAc modification. Oncol Rep 40: 2193-2205, 2018.
15. Khongmanee A, Lirdprapamongkol K, Tit-oon P, Chokchaichamnankit D, Svasti J and Srisomsap C: Proteomic analysis reveals important role of 14-3-3sigma in anoikis resistance of cholangiocarcinoma cells. Proteomics 13: 3157-3166, 2013.
16. Lirdprapamongkol K, Sakurai H, Kawasaki N, Choo MK, Saitoh Y, Aozuka Y, Singhirunnusorn P, Ruchirawat S, Svasti J and Saiki I: Vanillin suppresses in vitro invasion and in vivo metastasis of mouse breast cancer cells. Eur J Pharm Sci 25: 57-65, 2005.
17. Tit-Oon P, Chokchaichamnankit D, Khongmanee A, Sawangareetrakul P, Svasti J and Srisomsap C: Comparative secretome analysis of cholangiocarcinoma cell line in three-dimensional culture. Int J Oncol 45: 2108-2116, 2014.
18. Gasteiger E, Gattiker A, Hoogland C, Ivanyi I, Appel RD and Bairoch A: ExPASy: The proteomics server for in-depth protein knowledge and analysis. Nucleic Acids Res 31: 3784-3788, 2003.
19. Kall L, Canterbury JD, Weston J, Noble WS and MacCoss MJ: Semi-supervised learning for peptide identification from shotgun proteomics datasets. Nat Methods 4: 923-925, 2007.
20. O'Donnell N, Zachara NE, Hart GW and Marth JD: Ogt-dependent X-chromosome-linked protein glycosylation is a requisite modification in somatic cell function and embryo viability. Mol Cell Biol 24: 1680-1690, 2004.
21. Gu Y, Mi W, Ge Y, Liu H, Fan Q, Han C, Yang J, Han F, Lu X and Yu W: GlcNAcylation plays an essential role in breast cancer metastasis. Cancer Res 70: 6344-6351, 2010.
22. Lynch TP, Ferrer CM, Jackson SR, Shahriari KS, Vosseller K and Reginato MJ: Critical role of O-Linked beta-N-acetylglucosamine transferase in prostate cancer invasion, angiogenesis, and metastasis. J Biol Chem 287: 11070-11081, 2012.
23. Niu Y, Xia Y, Wang J and Shi X: O-GlcNAcylation promotes migration and invasion in human ovarian cancer cells via the RhoA/ROCK/MLC pathway. Mol Med Rep 15: 2083-2089, 2017.
24. Jiang M, Xu B, Li X, Shang Y, Chu Y, Wang W, Chen D, Wu N, Hu S, Zhang S, *et al*: O-GlcNAcylation promotes colorectal cancer metastasis via the miR-101-O-GlcNAc/EZH2 regulatory feedback circuit. Oncogene 38: 301-316, 2019.
25. Liu Q, Zhang H, Jiang X, Qian C, Liu Z and Luo D: Factors involved in cancer metastasis: A better understanding to 'seed and soil' hypothesis. Mol Cancer 16: 176, 2017.
26. Kim YN, Koo KH, Sung JY, Yun UJ and Kim H: Anoikis resistance: An essential prerequisite for tumor metastasis. Int J Cell Biol 2012: 306879, 2012.
27. Choi HS, Choi BY, Cho YY, Mizuno H, Kang BS, Bode AM and Dong Z: Phosphorylation of histone H3 at serine 10 is indispensable for neoplastic cell transformation. Cancer Res 65: 5818-5827, 2005.
28. Fong JJ, Nguyen BL, Bridger R, Medrano EE, Wells L, Pan S and Sifers RN: β-N-Acetylglucosamine (O-GlcNAc) is a novel regulator of mitosis-specific phosphorylations on histone H3. J Biol Chem 287: 12195-12203, 2012.
29. Phoomak C, Park D, Silsirivanit A, Sawanyawisuth K, Vaeteewoottacharn K, Detarya M, Wongkham C, Lebrilla CB and Wongkham S: O-GlcNAc-induced nuclear translocation of hnRNP-K is associated with progression and metastasis of cholangiocarcinoma. Mol Oncol 13: 338-357, 2019.
30. Wong JCT, Hasan MR, Rahman M, Yu AC, Chan SK, Schaeffer DF, Kennecke HF, Lim HJ, Owen D and Tai IT: Nucleophosmin 1, upregulated in adenomas and cancers of the colon, inhibits p53-mediated cellular senescence. Int J Cancer 133: 1567-1577, 2013.
31. Zeng D, Xiao YS, Zhu JL, Peng CY, Liang W and Lin HY: Knockdown of nucleophosmin 1 suppresses proliferation of triple-negative breast cancer cells through activating CDH1/Skp2/p27kip1 pathway. Cancer Manag Res 11: 143-156, 2019.
32. Qin FX, Shao HY, Chen XC, Tan S, Zhang HJ, Miao ZY, Wang L, Hui-Chen and Zhang L: Knockdown of NPM1 by RNA interference inhibits cells proliferation and induces apoptosis in leukemic cell line. Int J Med Sci 8: 287-294, 2011.
33. Kazemi Z, Chang HN, Haserodt S, McKen C and Zachara NE: O-linked beta-N-acetylglucosamine (O-GlcNAc) regulates stress-induced heat shock protein expression in a GSK-3beta-dependent manner. J Biol Chem 285: 39096-39107, 2010.
34. Hung CS, Huang CY, Lee CH, Chen WY, Huang MT, Wei PL and Chang YJ: IGFBP2 plays an important role in heat shock protein 27-mediated cancer progression and metastasis. Oncotarget 8: 54978-54992, 2017.
35. Cordonnier T, Bishop JL, Shiota M, Nip KM, Thaper D, Vahid S, Heroux D, Gleave M and Zoubeidi A: Hsp27 regulates EGF/β-catenin mediated epithelial to mesenchymal transition in prostate cancer. Int J Cancer 136: E496-E507, 2015.
36. Gibert B, Eckel B, Gonin V, Goldschneider D, Fombonne J, Deux B, Mehlen P, Arrigo AP, Clézardin P and Diaz-Latoud C: Targeting heat shock protein 27 (HspB1) interferes with bone metastasis and tumour formation in vivo. Brit J Cancer 107: 63-70, 2012.
37. Xiong XP, Vogler G, Kurthkoti K, Samsonova A and Zhou R: SmD1 modulates the miRNA pathway independently of its pre-mrna splicing function. PLoS Genet 11: e1005475, 2015.
38. Li Z and Pützer BM: Spliceosomal protein E regulates neoplastic cell growth by modulating expression of cyclin E/CDK2 and G2/M checkpoint proteins. J Cell Mol Med 12: 2427-2438, 2008.
39. Kim YD, Lee J, Kim HS, Lee MO, Son MY, Yoo CH, Choi JK, Lee SC and Cho YS: The unique spliceosome signature of human pluripotent stem cells is mediated by SNRPA1, SNRPD1, and PNN. Stem Cell Res 22: 43-53, 2017.
40. Quidville V, Alsafadi S, Goubar A, Commo F, Scott V, Pioche-Durieu C, Girault I, Baconnais S, Le Cam E, Lazar V, *et al*: Targeting the deregulated spliceosome core machinery in cancer cells triggers mTOR blockade and autophagy. Cancer Res 73: 2247-2258, 2013.
41. Hare SH and Harvey AJ: mTOR function and therapeutic targeting in breast cancer. Am J Cancer Res 7: 383-404, 2017.
42. Xu K, Liu P and Wei W: mTOR signaling in tumorigenesis. Biochim Biophys Acta 1846: 638-654, 2014.
43. Tian T, Li X and Zhang J: mTOR signaling in cancer and mTOR inhibitors in solid tumor targeting therapy. Int J Mol Sci 20: E755, 2019.
44. Malaguti P, Vari S, Cognetti F and Fabi A: The Mammalian target of rapamycin inhibitors in breast cancer: Current evidence and future directions. Anticancer Res 33: 21-28, 2013.
45. Liu J, Li HQ, Zhou FX, Yu JW, Sun L and Han ZH: Targeting the mTOR pathway in breast cancer. Tumour Biol 39: 1010428317710825, 2017.
46. Zaytseva YY, Valentino JD, Gulhati P and Evers BM: mTOR inhibitors in cancer therapy. Cancer Lett 319: 1-7, 2012.
47. Gomez-Pinillos A and Ferrari AC: mTOR signaling pathway and mTOR inhibitors in cancer therapy. Hematol Oncol Clin North Am 26: 483-505, vii, 2012.
48. Pópulo H, Lopes JM and Soares P: The mTOR signalling pathway in human cancer. Int J Mol Sci 13: 1886-1918, 2012.